



HHS Public Access

Author manuscript

Neuroimage. Author manuscript; available in PMC 2016 March 07.

Published in final edited form as:

Neuroimage. 2015 February 1; 106: 55–71. doi:10.1016/j.neuroimage.2014.11.009.

Subspecialization in the human posterior medial cortex

Danilo Bzdok^{1,2}, Adrian Heeger², Robert Langner^{1,2}, Angela R. Laird³, Peter T. Fox⁴, Nicola Palomero-Gallagher¹, Brent A. Vogt^{1,5}, Karl Zilles^{1,6}, and Simon B. Eickhoff^{1,2,*}

¹Institute of Neuroscience and Medicine (INM-1), Research Center Jülich, Jülich, Germany

²Institute of Clinical Neuroscience and Medical Psychology, Heinrich Heine University Düsseldorf, Düsseldorf, Germany

³Dept. of Physics, Florida International University, USA

⁴Research Imaging Institute, University of Texas Health Science Center, San Antonio, TX, USA

⁵Cingulum NeuroSciences Institute and Boston University School of Medicine, 72 E. Concord Street, Boston, MA 02118, USA

⁶Department of Psychiatry, Psychotherapy and Psychosomatics. RWTH Aachen University, 52074 Aachen, Germany

Abstract

The posterior medial cortex (PMC) is particularly poorly understood. Its neural activity changes have been related to highly disparate mental processes. We therefore investigated PMC properties with a data-driven exploratory approach. First, we subdivided the PMC by whole-brain coactivation profiles. Second, functional connectivity of the ensuing PMC regions was compared by task-constrained meta-analytic coactivation mapping (MACM) and task-unconstrained resting-state correlations (RSFC). Third, PMC regions were functionally described by forward/reverse functional inference. A precuneal cluster was mostly connected to the intraparietal sulcus, frontal eye fields, and right temporo-parietal junction; associated with attention and motor tasks. A ventral posterior cingulate cortex (PCC) cluster was mostly connected to the ventromedial prefrontal cortex and middle left inferior parietal cortex (IPC); associated with facial appraisal and language tasks. A dorsal PCC cluster was mostly connected to the dorsomedial prefrontal cortex, anterior/posterior IPC, posterior midcingulate cortex, and left dorsolateral prefrontal cortex; associated with delay discounting. A cluster in the retrosplenial cortex was mostly connected to the anterior thalamus and hippocampus. Furthermore, all PMC clusters were congruently coupled with the default mode network according to task-constrained but not task-unconstrained connectivity. We thus identified distinct regions in the PMC and characterized their neural networks and functional implications.

*Correspondence should be addressed to: Prof. Dr. Simon Eickhoff, Institut für Neurowissenschaften und Medizin (INM-1), Forschungszentrum Jülich GmbH, D-52425 Jülich, Germany, Phone: +49 2461 61-8609, Fax: +49 2461 61-2820, S.Eickhoff@fz-juelich.de.

Publisher's Disclaimer: This is a PDF file of an unedited manuscript that has been accepted for publication. As a service to our customers we are providing this early version of the manuscript. The manuscript will undergo copyediting, typesetting, and review of the resulting proof before it is published in its final citable form. Please note that during the production process errors may be discovered which could affect the content, and all legal disclaimers that apply to the journal pertain.

Keywords

connectivity-based parcellation; statistical learning; functional decoding; parietal lobe; posterior cingulate cortex; retrosplenial cortex; default mode network

Introduction

The human posterior medial cortex (PMC) has been functionally implicated in tasks as diverse as attention, memory, spatial navigation, emotion, self-relevance detection, and reward evaluation. The PMC relates to the ventral and dorsal posterior cingulate cortex (vPCC and dPCC; areas 23 and 31), retrosplenial cortex (RSC; areas 29 and 30), and precuneus (PrC; area 7M, Scheperjans et al., 2008b). While the PCC and RSC belong to the cingulate cortex, the PrC belongs to the parietal lobe (Vogt et al., 2006). The RSC is located ventrocaudal to the splenium of the ventral bank of the corpus callosum. This brain region forms a belt in the callosal sulcus around the splenium. That is, the RSC is located on the ventral bank of the cingulate gyrus and only emerges slightly onto the cortical surface, mostly at ventrocaudal portions (Vogt et al., 2001). The PrC is the continuation of the superior parietal lobule on the medial hemispheric surface and abuts the dorsocaudal PCC. The PCC is located between RSC and PrC, caudal to the midcingulate cortex as well as dorsal, caudal, and ventral to the splenium. Although the RSC, PrC, and PCC have substantially different cytoarchitectures and task-related functions, they have each been implicated in the default mode network; hence the notion of an overarching PMC supregion. Figure 1 shows these four regions in a neuroanatomical scheme, while figure 2 shows them as a combined supregion.

The organization of the PMC was recently addressed using resting-state-correlation-based parcellation in monkeys and humans (Margulies et al., 2009). The regional functional connectivity patterns converged across species to a sensorimotor role for the anterior precuneus (i.e., dorsal PMC along the marginal ramus), a cognitive/associative role for the central precuneus (i.e., dorsocaudal PMC), a more visual role for the posterior precuneus (dorsal to the parieto-occipital sulcus), and a limbic role for the PCC/RSC (i.e., rostroventral PMC). Importantly, Margulies et al. also provided evidence that the PCC, but not precuneus, is an integral part of the so-called default mode network. Furthermore, all portions of the PMC were strongly interconnected (local interconnections being relatively strongest) as investigated using different antero- and retrograd tracers in monkeys (Parvizi et al., 2006). Yet, PCC and precuneus regions within the PMC were, for instance, distinguishable by the strength of (para-)hippocampal connections. The retrosplenial PCC concurrently dominated in connectivity to limbic networks for emotion processing, whereas the precuneal area 7m concurrently featured specific connectivity to cingulo-frontal networks for action execution. The particularly diverse connectivity targets of the dorsocaudal PCC could speak in favor of either a distinctive property or a transitory area (by its location between areas 31 and 23). Parvizi et al. concluded that globally strong intra-PMC connectivity together with locally distinct extra-PMC connectivity might indicate realization of supregion computational goals emerging from collaboration between PMC components. More specifically, neuroanatomists (Vogt, 2005; Vogt et al., 2006) advocated duality in the PCC with a dorsal

component (including dorsal areas 23a/b/c and adjacent rostral area 31), frequently related to body-in-space cognition, and a ventral component (including ventral areas 23a/b and adjacent caudal area 31), frequently related to self/emotional relevance cognition vis-à-vis objects. Moreover, resting-state-derived (Zhang and Li, 2012) and DTI-derived (Zhang et al., 2014) parcellations of the PMC provided evidence for a possible functional subspecialization within the precuneus of the PMC.

Perhaps due to the PMC's mosaic organization, attempts of global functional accounts range from covert reallocation of spatial attention (Gitelman et al., 1999), mediation between internal and external focus (Leech and Sharp, 2014), computation of environmental statistics (Pearson et al., 2009), and self-referential visuospatial imagery (Cavanna and Trimble, 2006) to modality-independent integration between emotional states and memories (Maddock, 1999). These proposed *domain-spanning* roles potentially explain its various *domain-specific* functional involvements, such as visual rotation, deductive reasoning, autobiographical memory retrieval, and mental navigation in space. As a consequence of overarching functions, the PMC is consistently implicated in a variety of major psychiatric disorders, including schizophrenia, depression, autism, and ADHD (Leech and Sharp, 2014; Whitfield-Gabrieli and Ford, 2012).

Besides the uncertainty associated with its alleged functional roles (cf. Cavanna and Trimble, 2006), the human and non-human primate PMC stands out in a number of studies of brain metabolism, electrophysiologically recorded activity, and myelogenesis. Metabolically, the PMC has the highest level of basal glucose energy consumption in humans (Gusnard and Raichle, 2001) and other species (Harley and Bielajew, 1992; Matsunami et al., 1989). (Patho-)Physiologically, metabolic fluctuations in the human PMC have been closely related to various instances of altered conscious awareness, including anesthesia (Fiset et al., 1999), sleep (Maquet, 2000), and restoration from vegetative states (Laureys et al., 1999). Electrophysiologically, gamma band recordings in humans (Dastjerdi et al., 2011) and single-cell recordings in monkeys (Hayden et al., 2009) revealed activity *reductions* in the PMC during attentionally demanding tasks compared to rest. Functionally, such activity patterns in the absence of a defined task have long been speculated to reflect constant contemplation of (external) environment and (internal) memory (cf. Berger, 1931; Ingvar, 1979; Vogt et al., 1992). It is noteworthy that the PMC has, however, no direct connections with primary sensory regions (Cavanna and Trimble, 2006; Leech and Sharp, 2014; Parvizi et al., 2006), but has been described as a network “hub” exhibiting high centrality in graphanalytical examination (Hagmann et al., 2008). Finally, axons in parts of the PMC myelinate comparatively late during postnatal development in monkeys (Goldman-Rakic, 1987). Such late postnatal myelination is generally believed to occur in the phylogenetically most developed “associations” regions (Flechsig, 1920), thus mimicking the phylogenetic brain development during ontogeny (Couch et al., 2007). Taken together, we know that the PMC has numerous exceptional neurobiological properties. Nevertheless, the precise nature of neural processes realized in that part of the brain remains as elusive as its neurobiological organization.

We here aimed at a multi-modal characterization of the organization, connectivity, and function of the PMC suprapregion. To this end, we used a data-driven approach that extracts

structured knowledge emerging from several hundreds of neuroimaging studies (Hastie et al., 2011). First, we performed connectivity-based parcellation (Eickhoff et al., 2011; Johansen-Berg et al., 2004) of a volume of interest (VOI) comprising those portions of PCC, RSC, and PrC that are located within the PMC. This analysis tested whether local differences in whole-brain meta-analytic connectivity-modeling (MACM) enable identification of distinct regions within the PMC (cf. Cauda et al., 2010; Leech and Sharp, 2014; Margulies et al., 2009; Zhang et al., 2014). Second, the ensuing connectivity-derived regions were characterized by two measures of functional connectivity (cf. Cauda et al., 2011; Chang et al., 2013): the identical MACM approach, capturing brain activity in experimental settings, but also resting-state functional connectivity (RSFC), capturing brain activity in the absence of an experimental paradigm. This analysis thus tested what remote parts of the brain interact with the connectivity-derived regions congruently in the presence and absence of defined psychological tasks. Third, we delineated the derived regions' functional profiles by reference to the extensive meta-data in the BrainMap database (Fox and Lancaster, 2002) using quantitative forward and reverse inference. This last analysis tested whether regions in the PMC are more robustly associated with any taxonomic task descriptions than would be expected by chance. These investigations provided a statistically defensible characterization of subdivisions, connectivity, and function of the PMC supraregion making a minimum of a priori assumptions.

Material and Methods

Defining the volume of interest

The volume of interest (VOI) comprising the PMC was defined using neuroanatomical landmarks. Cytoarchitectonic information provided the superior borders, while macroanatomical structures of the MNI (Montreal Neurological Institute) standard brain guided the delineation of most other borders as described below.

Regarding the superior borders of the VOI, topographical information was provided by histological probability maps from the Jülich brain atlas (Zilles and Amunts, 2010). Based on regionally specific appearance of cortical layers, cell density, and cell types, the human cortex can be divided into a large number of cytoarchitectonically distinct brain regions. This structural segregation is an important indicator of functional heterogeneity. More specifically, the posterosuperior extent of the VOI was limited by the borders of the cytoarchitectonic areas 5M (yellow line), 7A (red line), and 7P (green line) (Scheperjans et al., 2008b). Regarding the anterosuperior border, the VOI was drawn such as to border the dysgranular area 23d (blue line), as indicated by Vogt and colleagues (2006). For the remaining VOI borders, obvious macroanatomical structures served as topographical landmarks, including the splenium of the corpus callosum (purple curved line, defining the rostral VOI border) and the parietooccipital sulcus (pink line, defining the ventral VOI border). This neuroanatomically defined supraregion of interest including the gray-matter of the PrC, PCC, and RSC within the PMC (Fig. 2) served as the basis for all subsequent analyses.

Workflow Overview

First, meta-analytic connectivity modeling (MACM) was used to determine the coactivation profile of each voxel within the VOI. The seed voxels were then grouped based on similarities of their coactivation profiles by *k*-means clustering. The most stable clustering solution was identified by the combination of different cluster stability metrics. Second, the whole-brain connectivity patterns of each derived cluster in the VOI were determined based on MACM and resting-state functional connectivity (RSFC). Third, the functional profiles of the ensuing clusters were determined by testing for significant overrepresentation of taxonomic classes of the BrainMap database, which describe psychological and experimental properties of each stored neuroimaging study. These steps incorporated a data-guided framework to comprehensively characterize the PMC.

Meta-analytic connectivity modeling

Delineation of whole-brain coactivation maps for each voxel of the PMC seed region was performed based on the BrainMap database (www.brainmap.org; Fox and Lancaster, 2002; Laird et al., 2011b). We constrained our analysis to fMRI (functional magnetic resonance imaging) and PET (positron emission tomography) experiments from conventional mapping (no interventions, no group comparisons) in healthy participants, which reported results as coordinates in stereotaxic space. These inclusion criteria yielded $\sim 7,500$ eligible experiments at the time of analysis (queried in October 2012). Note that we considered all eligible BrainMap experiments because any pre-selection based on taxonomic categories would have constituted a strong a priori hypothesis about how brain networks are organized. However, it remains elusive how well psychological constructs, such as emotion and cognition, map on regional brain responses (Laird et al., 2009a; Mesulam, 1998; Poldrack, 2006).

The aim of the coactivation analysis is to determine the spatial convergence of neural activity across all foci of all BrainMap experiments in which the seed voxel in question is reported as active. However, a challenge in constructing voxel-wise coactivation maps is the limited number of experiments activating precisely at any particular seed voxel. Hence, pooling across the close spatial neighborhood has become the dominant approach in MACM analysis (Eickhoff et al., 2011) to enable a reliable delineation of task-based functional connectivity. Importantly, the extent of this spatial filter was systematically varied from including the closest 20 to 200 experiments in steps of five (Clos et al., 2013). That is, we selected the sets of 20, 25, 30, 35, ..., 200 experiments reporting the closest activation at a given seed voxel (i.e., 37 filter sizes). This was achieved by calculating and subsequently sorting the Euclidean distances between a given seed voxel and any activation reported in BrainMap. Then, the nearest activation foci (number of foci indicated by the filter size) were associated with that seed voxel.

Notably, the association of a seed voxel with experiments by either constraining the maximum experiment count or constraining the maximum distance between seed voxel and nearest experiment focus have been demonstrated to yield highly comparable results (Eickhoff et al., 2011). We here opted for a maximum-experiment-count constraint, rather than a maximum-distance constraint. This is because the number of experiments associated

with a seed voxel has a considerable influence on the ensuing whole-brain maps. Unbalanced numbers of experiment across seed voxels would then disadvantageously affect clustering based on the seed-voxel whole-brain connectivity maps. In other words, the ensuing clustering of the VOI would be strongly driven by unequal sizes of the seed voxels' experiment sets, rather than their actual whole-brain connectivity patterns. Additionally, choosing a radius constraint would be disadvantageous in yielding lower resolution in parts of the brain that are sparsely populated by activating BrainMap experiments.

The retrieved experiments were then used to compute the brain-wide coactivation profile of a given seed voxel for each of the 37 filter sizes. In particular, we performed a coordinate-based meta-analysis over all foci reported in these experiments to quantify their convergence. Since the experiments were identified by activation in or near a particular seed voxel, convergence was always highest at the location of the seed. Convergence outside the seed, however, indicated coactivation across task-based functional neuroimaging experiments.

These brain-wide coactivation patterns for each individual seed voxel were computed by activation likelihood estimation (ALE). The key idea behind ALE is to treat the foci reported in the associated experiments not as single points, but as centers for 3D Gaussian probability distributions that reflect the spatial uncertainty associated with neuroimaging results. Using the latest ALE implementation (Eickhoff et al., 2012; Eickhoff et al., 2009; Turkeltaub et al., 2012), the spatial extent of those Gaussian probability distributions was based on empirical estimates of between-participant and between-template variance of neuroimaging foci (Eickhoff et al., 2009). For each experiment, the probability distributions of all reported foci were then combined into a modeled activation (MA) map by the recently introduced “non-additive” approach that prevents local summation effects (Turkeltaub et al., 2012). The voxel-wise union across the MA maps of all experiments associated with the current seed voxel then yielded an ALE score for each voxel of the brain that describes the coactivation probability of that particular location with the current seed voxel. The ALE scores of all voxels within gray matter (based on 10% probability according to the ICBM maps) were recorded before moving to the next voxel of the seed region.

In sum, quantitative ALE meta-analysis over all foci reported in the experiments associated with the current seed voxel determined how likely any other voxel throughout the brain was to coactivate with that particular seed voxel. Note that no threshold was applied to the ensuing coactivation maps at this point of analysis to retain the complete pattern of coactivation likelihood.

Connectivity-based parcellation

The unthresholded brain-wide coactivation profiles for all seed voxels were then combined into a $N_S \times N_T$ coactivation matrix, where N_S denotes the number of seed voxels (5198 voxels in the present VOI) and N_T the number of target voxels in the gray matter of the reference brain volume at $4 \times 4 \times 4 \text{ mm}^3$ resolution ($\sim 30,000$ voxels located within gray matter). Given the use of 37 different filter sizes, this step resulted in 37 individual coactivation matrices, each representing the whole-brain connectivity of the seed voxels at a particular filter size. The parcellation of the VOI was performed using k -means clustering as

implemented in Matlab with $k = 2, 3, \dots, 9$ using one minus the correlation between the connectivity patterns of seed voxels as a distance measure (i.e., correlation distance). k -means clustering is a non-hierarchical clustering method that uses an iterative algorithm to separate the seed region into a previously selected number of k non-overlapping clusters (Forgy, 1965; Hartigan and Wong, 1979). Clustering using the k -means algorithm consists in minimizing the variance within clusters and maximizing the variance between clusters by first computing the centroid of each cluster and subsequently reassigning voxels to the clusters such that their difference from the nearest centroid is minimal. This parcellation was performed for each of the 37 filter sizes independently, yielding 8 (k means cluster solutions) \times 37 (filter size) independent cluster solutions. For each of the 8×37 parcellations we recorded the best solutions from 25 replications with randomly placed initial centroids. This procedure is necessary as k -means clustering is known to potentially yield different results (local minima) depending on the random initial position of the cluster centroids (Nanetti et al., 2009). Repeating computation of the same clustering problem 25 times therefore allowed delineation of the most robust clustering solutions for a given number of clusters.

Selection of optimal filter range

For each of the 37 filter sizes, the k -means procedure thus yielded eight different solutions parcellating the PMC into two, three, ... up to nine subdivisions. One of the well-known challenges of data clustering in neuroinformatics and computer science in general is the choice of an “optimal” cluster solution. This problem is further complicated in the current MACM-based parcellation approach because not only the optimal number of clusters k had to be determined, but also the use of multiple spatial filter sizes. In previous parcellation studies involving MACM and multiple filter sizes this issue was addressed by averaging *across all filter sizes* (Bzdok et al., 2012a; Cieslik et al., 2012). As an improvement over this previous approach, we here used a recently introduced two-step procedure that involves a first decision on those filter sizes (i.e., the target range) to be included in the final analysis and a second decision on the optimal cluster solution (Clos et al., 2013). That is, we first examined the properties of each filter size across all cluster solutions and isolated *the most stable range of filter sizes*. These were then submitted to further analysis. This first step was based on the consistency of the cluster assignments for the individual voxels across the different filter sizes and selecting the filter range with the lowest number of deviants, i.e., voxels that were assigned differently as compared to the solution from the majority of filters. In other words, we identified those filter sizes that reflected solutions most similar to the consensus solution. Comparing the number of deviant cluster assignments (i.e., the number of times a given voxel was assigned to another than the majority cluster; normalized for k) indicated that most deviants were present in parcellations based on small but also very large filter sizes. The filter size range was chosen (90 to 155) based on the increase in the weighted sum (across all k) of the z -normalized number of deviant before and after these values (cut off at $z < -0.5$: only those filter sizes were included where the number of deviants was at least half a standard-deviation lower than the average number of deviants across all filter sizes). In all subsequent steps, the analysis was thus restricted to the parcellations based on coactivation as estimated from the nearest 90 to 155 experiments.

Selection of the optimal number of clusters

We subsequently determined *the optimal solution of k clusters* (restricted to the 14 selected filter sizes as outlined in the last paragraph). This was indicated by majority vote of four different criteria describing information-theoretic, cluster-separation, and topological properties of the various cluster solutions.

First, as an information-theoretic criterion, we assessed the similarity of cluster assignments within the current solution (k) for the various filter sizes, by computing the variation of information (VI) (Meila, 2007), to subsequently juxtapose robustness of the k -th solution with that of the neighboring ($k-1$ and $k+1$) solutions. The VI metric has been previously used for selecting the best fitting k -means parcellation model of a given brain region by Kelly et al. (2010) and Kahnt et al. (2012). The variation of information between two cluster solutions C and C' (i.e., same number of clusters but different filter sizes) was computed by

$$VI(C, C')_k = H(C)_k + H(C')_k - 2I(C, C')_k$$

where H represents the amount of information (entropy) present in the cluster solutions C and C' and I represents the mutual information shared by the two cluster solutions C and C' . For each PMC parcellation solution of k clusters, the VI was computed for and averaged across different variants of parameter choices (i.e., filter size) to see whether the cluster solution is more robust than its neighboring ($k-1$) and ($k+1$) solutions. Solutions were considered stable either if there was an increase in VI from the current to the subsequent set of solutions (primary criterion) or if there was a decrease from the previous to the current clustering step (secondary criterion).

Second, as a cluster-separation criterion, the silhouette coefficient (Kaufman and Rousseeuw, 1990) is a general measure of how similar a given voxel is to voxels in its own cluster compared to voxels in other clusters (averaged across voxels of a given filter size). This coefficient ranges from -1 to $+1$. Good solutions are those with a higher silhouette value compared to the $k-1$ solution (primary criterion) or whose silhouette coefficient is at least not decreased compared to the previous $k-1$ solution (secondary criterion).

Third, as another cluster-separation criterion, the change in inter- versus intra-cluster distance ratio was computed (Chang et al., 2009). That is, the first derivative of the ratio between the average distance of a given voxel to its own cluster center and the average distance between the cluster centers. This ratio has the tendency to decrease with increasing number of clusters. This is why deviation from this behavior is believed to be an indicator of particularly good model fit of the current clustering solution. In other words, an increased ratio compared to the $k-1$ solution indicates a better separation of the obtained clusters. Good solutions are those for which the subsequent $k+1$ solution does not show a much larger increase in the inter-cluster versus intra-cluster ratio.

Fourth, as a topological criterion, we considered the percentage of misclassified voxels (deviants) across filter sizes of a given cluster solution. This criterion indirectly reflects the amount of noise and potentially local effects in the clustering. In particular, the criterion

addresses the across-filter stability, that is, the average percentage of voxels for each filter size that were assigned to a different cluster, as compared to the most frequent assignment of these voxels across all filter sizes. Those k parcellations were considered good solutions whose percentages of deviants (presumably reflecting noise and local variance) were not increased compared to the $k-1$ solution and, in particular, if the subsequent $k+1$ solution led to a higher percentage of deviants.

These four different criteria estimating cluster stability conjointly allowed for an objective, cross-validated identification of the cluster solution with the highest within-cluster homogeneity and between-cluster heterogeneity based on seed-voxel-wise whole brain connectivity.

Characterization of the clusters: task-dependent connectivity

To determine the significant functional connectivity of the derived *clusters*, another meta-analytic connectivity modeling analysis (MACM) was performed. In the first step, we identified all experiments in the BrainMap database that featured at least one focus of activation in a particular cluster (derived from the coactivation-based parcellation). That is, in contradistinction to the above MACM analyses, we did not select experiments activating at or close to a particular voxel but rather all those that activated in one of the CBP-derived clusters. Next, ALE meta-analysis was performed on these experiments as described above. In contrast to the MACM underlying the CBP, in which ALE maps were not thresholded to retain the complete pattern of coactivation likelihoods, statistical inference was now performed. To establish which brain regions were significantly coactivated with a given cluster, ALE scores for the MACM analysis of this cluster were compared to a null-distribution reflecting a random spatial association between experiments with a fixed within-experiment distribution of foci (Eickhoff et al., 2009). This random-effects inference assesses above-chance convergence across experiments, not clustering of foci within a particular experiment. The observed ALE scores from the actual meta-analysis of experiments activating within a particular cluster were then tested against ALE scores obtained under a null-distribution of random spatial association yielding a p-value based on the proportion of equal or higher random values (Eickhoff et al., 2012). The resulting non-parametric p-values were transformed into z-scores and thresholded at a cluster-level corrected threshold of $p < 0.05$ (cluster-forming threshold at voxel-level $p < 0.001$).

Differences in coactivation patterns between the identified clusters were tested by performing MACM separately on the experiments associated with either cluster and computing the voxel-wise difference between the ensuing ALE maps. All experiments contributing to either analysis were then pooled and randomly divided into two groups of the same size as the two original sets of experiments defined by activation in the first or second cluster (Eickhoff et al., 2012). ALE-scores for these two randomly assembled groups, reflecting the null-hypothesis of label exchangeability, were calculated and the difference between these ALE-scores was recorded for each voxel in the brain. Repeating this process 10,000 times then yielded a voxel-wise null-distribution of the differences in ALE-scores between the MACM analyses of the two clusters. The ‘true’ differences in ALE scores were then tested against this null-distribution yielding a p-value for the difference at each voxel

based on the proportion of equal or higher differences under the condition of label exchangeability. The resulting non-parametric p-values were thresholded at $P > 0.95$ (95% chance of a true difference), transformed into z-scores, and inclusively masked by the respective main effects (i.e., the significant effects in the MACM for a given cluster). Finally, we computed the specific coactivation pattern for all clusters, that is, brain regions significantly more coactivated with a given cluster than with any of the other ones. This specific cluster-wise coactivation pattern was computed by performing a conjunction analysis across all difference maps obtained from contrasting the given cluster with each remaining one.

Characterization of the clusters: task-independent connectivity

Significant clusters-wise whole-brain connectivity was likewise assessed using resting-state correlations as an independent modality of functional connectivity for cross-validation across disparate brain states. RSFC fMRI images were obtained from the Nathan Kline Institute Rockland-sample, which are available online as part of the International Neuroimaging Datasharing Initiative (http://fcon_1000.projects.nitrc.org/indi/pro/nki.html). In total, the processed sample consisted of 132 healthy participants between 18 and 85 years (mean age: 42.3 ± 18.08 years; 78 male, 54 female) with 260 echo-planar imaging (EPI) images per participant. Images were acquired on a Siemens TrioTim 3T scanner using blood-oxygen-level-dependent (BOLD) contrast [gradient-echo EPI pulse sequence, repetition time (TR) = 2.5 s, echo time (TE) = 30 ms, flip angle = 80° , in-plane resolution = 3.0×3.0 mm, 38 axial slices (3.0 mm thickness), covering the entire brain]. The first four scans served as dummy images allowing for magnetic field saturation and were discarded prior to further processing using SPM8 (www.fil.ion.ucl.ac.uk/spm). The remaining EPI images were then first corrected for head movement by affine registration using a two-pass procedure. The mean EPI image for each participant was spatially normalized to the MNI single-subject template (Holmes et al., 1998) using the ‘unified segmentation’ approach (Ashburner and Friston, 2005). The ensuing deformation was then applied to the individual EPI volumes. Finally, images were smoothed by a 5-mm FWHM Gaussian kernel to improve signal-to-noise ratio and account for residual anatomical variations.

The time-series data of each individual seed voxel were processed as follows (Fox et al., 2009; Weissenbacher et al., 2009): In order to reduce spurious correlations, variance that could be explained by the following nuisance variables was removed: (i) The six motion parameters derived from the image realignment, (ii) the first derivative of the realignment parameters, and (iii) mean gray matter, white matter, and CSF signal per time point as obtained by averaging across voxels attributed to the respective tissue class in the SPM 8 segmentation (Reetz et al., 2012). All of these nuisance variables entered the model as first- and second-order terms (Jakobs et al., 2012). Data were then band-pass filtered preserving frequencies between 0.01 and 0.08 Hz since meaningful resting-state correlations will predominantly be found in these frequencies given that the BOLD-response acts as a low-pass filter (Biswal et al., 1995; Fox and Raichle, 2007).

To measure cluster-wise task-independent connectivity, time courses were extracted for all gray-matter voxels of a given cluster. The cluster time course was then expressed as the first eigenvariate of these voxels' time courses. Pearson correlation coefficients between the time series of the CBP-derived PMC clusters and all other gray-matter voxels in the brain were computed to quantify RSFC. These voxel-wise correlation coefficients were then transformed into Fisher's Z-scores and tested for consistency across participants using a random-effects, repeated-measures analysis of variance. The main effect of connectivity for individual clusters and contrasts between those were tested using the standard SPM8 implementations with the appropriate non-sphericity correction. The results of these random-effects analyses were cluster-level thresholded at $p < 0.05$ (cluster-forming threshold at voxel-level: $p < 0.001$), analogous to the MACM-based difference analysis. The specific resting-state correlations for a given cluster were then computed by performing a conjunction analysis across the differences between a given cluster and the remaining ones, analogous to the MACM-based cluster analyses above.

Characterization of the clusters: conjunction across connectivity types and clusters

To delineate brain regions showing task-dependent and task-independent functional connectivity with the derived clusters in the PMC, we performed a conjunction analysis of the MACM and RSFC results using the strict minimum statistics (Nichols et al., 2005).

In one approach, brain regions connected with *individual clusters* across both connectivity measures were delineated by computing the intersection of the (cluster-level family-wise-error-corrected) connectivity maps from the two connectivity analyses detailed above. In this way, each PMC cluster was associated with a network of brain regions that are congruently connected to that cluster across two disparate brain states, i.e., task-focused and mental operations in a task-free setting.

In a second approach, we tested, for MACM and RSFC *separately*, whether *all clusters* in the PMC are congruently functionally connected to other parts of the brain. That is, we performed a conjunction analysis across the (cluster-level family-wise-error-corrected) connectivity maps of all PMC clusters based on either MACM or RSFC. In this way, the task-focused and task-free brain states were characterized by congruent functional connectivity of all clusters in the PMC.

Characterization of the clusters: function

Finally, the CBP-derived clusters were individually submitted to an analysis of their functional profiles. It is important to note that this functional characterization constitutes a post-hoc procedure that is subsequent to and independent of the connectivity analyses. The functional characterization was based on the BrainMap meta-data that describe each neuroimaging experiment included in the database. Behavioral domains code the mental processes isolated by the statistical contrasts (Fox et al., 2005) and comprise the main categories of cognition, action, perception, emotion, and interoception, as well as their related sub-categories. Paradigm classes categorize the specific task employed (see <http://brainmap.org/scribe/for> the complete BrainMap taxonomy).

Forward inference on the functional characterization then tests the probability of observing activity in a brain region given knowledge of the psychological process, whereas *reverse inference* tests the probability of a psychological process being present given knowledge of activation in a particular brain region. Using forward inference, a cluster's functional profile was determined by identifying taxonomic labels for which the probability of finding activation in the respective cluster was significantly higher than the a priori chance (across the entire database) of finding activation in that particular cluster. Significance was established using a binomial test ($p < 0.05$; Eickhoff et al., 2011; Nickl-Jockschat et al., 2012). That is, we tested whether the conditional probability of activation given a particular label $P(\text{Activation}|\text{Task})$ was higher than the baseline probability of activating the brain region in question per se $P(\text{Activation})$. Using reverse inference, a cluster's functional profile was determined by identifying the most likely behavioral domains and paradigm classes given activation in a particular cluster. This likelihood $P(\text{Task}|\text{Activation})$ can be derived from $P(\text{Activation}|\text{Task})$ as well as $P(\text{Task})$ and $P(\text{Activation})$ using Bayes' rule. Significance was then assessed by means of a chi-square test ($p < 0.05$). In sum, forward inference assessed the probability of activation given a psychological term, while reverse inference assessed the probability of a psychological term given activation.

In the context of quantitative functional decoding, it is important to appreciate that this approach aims at relating defined psychological tasks to the examined brain regions instead of claiming “a unique role” of a brain region for any psychological processes and tasks (Poldrack, 2006; Yarkoni et al., 2011). Put differently, an association of task X to brain region Y obtained in these analyses does not necessarily imply that neural activity in brain region Y is *limited to* task X.

Results

Parcellation stability

Several metrics were applied to weigh the various cluster solutions for the PMC VOI against each other (Fig. 3). First, the information-theoretic criterion ‘variation of information’ slightly decreased from three to four clusters and steeply increased from four to five clusters. This indicated that each cluster of the k -means clusterings became increasingly chaotic starting from five clusters. Second, the cluster-separation criterion ‘silhouette coefficient’ showed a positive bump at four clusters in the upward trend starting from three clusters. This indicated that clustering into four groups featured unexpectedly compact clusters, although compactness increases with the number of clusters. Third, the other cluster-separation criterion change of ‘intercluster/intracluster ratio’ was highest for four clusters. This indicated that the four-cluster solution best isolated each cluster from the remaining ones. Fourth, as a topological criterion, the percentage of misclassified voxels across filter sizes was lowest for four clusters. This indicated that the four-cluster solution exhibited the least noise across the different filter sizes. The four different measures of clustering quality thus unequivocally advocated the four-cluster solution as the most robust differentiation in the PMC VOI. Moreover, in the four-cluster solution each PMC region consisted of a continuously classified volume (Fig. 4). The absence of voxel “enclaves” further attested to the methodological robustness and biological meaningfulness of the choice on four clusters.

Cluster topography

In the four-cluster solution, cluster 1 emerged in the dorsocaudal part of the VOI in the parietal lobe (Fig. 4). Cluster 2 emerged in the ventral part of the VOI in the posterior cingulate cortex (cf. Vogt et al., 2006). Cluster 3 emerged in the dorsorostral VOI in the posterior cingulate cortex, such as cluster 2. Finally, cluster 4 emerged in the ventrorostral VOI in and near to the retrosplenial cortex (cf. Vann et al., 2009). All four clusters were sagittally symmetric. This was assessed by quantifying the voxel-wise interhemispheric congruency of cluster 1 to 4, which yielded 81%, 79%, 91%, and 70%, respectively.

Individual cluster connectivity

We first assessed the cluster-level corrected meta-analytic coactivations (MACM) of each PMC cluster individually (Fig. 5 A). The minimum permissible number of continuously connected voxel (i.e., smallest significant cluster size) for cluster 1, 2, 3 and 4 were 186, 151, 101, and 15 voxels, respectively. Clusters 1, 2, and 3 were all connected to the bilateral inferior parietal cortex (IPC; cluster 1 was cytoarchitectonically assigned to: right areas PGa/PGp/PFm/PF and left areas PGa/PFm; cluster 2: bilateral PGp; cluster 3: bilateral PFm/PGa/PGp; Caspers et al., 2006), extending into the temporo-parietal junction (TPJ). For cluster 3, this convergent activation additionally extended into the left posterior superior temporal sulcus. Cluster 1 was also connected to the bilateral intraparietal sulcus (IPS; assigned to areas hIP1 and hIP3) and superior parietal cortex (SPC; areas 7A, 7M, 7P) (Scheperjans et al., 2008a; Scheperjans et al., 2008b), while cluster 3 was connected to the left IPS (assigned to areas hIP1 and hIP3) and left SPC. Cluster 1 was further connected to the bilateral caudate nucleus and right globus pallidus, while coactivation with these two brain regions were left-lateralized for clusters 2 and 3. Similarly, cluster 1 was connected to the bilateral dorsolateral prefrontal cortex (dlPFC), extending into the frontal eye field (FEF), while cluster 3 was connected only to the left dlPFC. Clusters 1 and 3 were both connected to the bilateral supplementary motor area (SMA) and midcingulate cortex (MCC). Clusters 1 and 3 also featured bilateral connectivity to the anterior insula, while cluster 2 featured connectivity only to the left anterior insula. Clusters 2 and 3 were both connected to the bilateral ventromedial and dorsomedial prefrontal cortex (vmPFC/dmPFC), including the frontal pole (FP; assigned to area FP2, Bludau et al., 2013) and pre/subgenual anterior cingulate cortex (ACC; cluster 3 extending into anterior MCC), while cluster 4 was (more weakly than clusters 2 and 3) connected to the bilateral vmPFC. Clusters 2 and 3 were also both connected to the bilateral hippocampus (assigned to subiculum and CA), while cluster 4 was connected to the right hippocampus (assigned to subiculum and CA). Only cluster 2 was connected to the bilateral amygdala (laterobasal and superficial nuclei groups; Amunts et al., 2005) as well as the left inferior frontal gyrus (IFG; area 45; Amunts et al., 1999) and left middle temporal gyrus (MTG). Clusters 1 and 4 were connected to the bilateral anterior thalamus (extending to middle and posterior nuclei for cluster 1), while cluster 2 was connected only to the left anterior thalamus.

After the task-dependent MACM analyses, we assessed the task-independent, cluster-level corrected resting-state correlations (RSFC) of each PMC cluster individually (Fig. 5 B). The minimally significant cluster sizes for cluster 1, 2, 3, and 4 were 11, 35, 22, and 89 voxels, respectively. All four clusters were connected to the bilateral vmPFC, FP (assigned to area

FP2), dmPFC, pre/subgenual ACC, anterior MCC, hippocampus (assigned to subiculum and CA, extending into the area of the entorhinal cortex), parahippocampal gyrus, inferior parietal cortex (assigned to areas PGa/PGp; clusters 2/3: additionally PFm), extending into the TPJ, IPS (assigned to areas hIP1/hIP3), superior parietal cortex (assigned to areas 7A/7P), posterior MCC (pMCC), MTG, temporal pole (except for cluster 4 on the left), dlPFC (extending into the FEF), thalamus, and cerebellum. Notably, cluster 4 showed by far the most prominent coupling with the occipital lobe (assigned to areas 17, 18, and hOCV3; Amunts et al., 2000). Clusters 2 and 4 showed connectivity extending to the bilateral amygdalae (assigned to laterobasal and superficial nuclei groups) and nucleus accumbens.

After separate MACM and RSFC analysis, we tested for congruent functional coupling across the presence and absence of task by a conjunction analysis of the above individual MACM and RSFC results of the PMC clusters (Fig. 5 C). All four clusters were congruently connected to the bilateral pMCC. Cluster 1 was congruently connected to the bilateral thalamus (more strongly on the left), FEF, TPJ (more strongly on the right), and IPS/SPC (assigned to areas hIP1, hIP3, and 7A) across MACM and RSFC. Both clusters 2 and 3 were congruently connected to the bilateral vmPFC, FP (assigned to area FP2), dmPFC, pregenual ACC, hippocampus (assigned to subiculum and CA), and IPC (cluster 2: assigned to bilateral PGp; cluster 3: assigned to bilateral PGa/PGp). Additionally, cluster 2 was congruently connected to the left nucleus accumbens, amygdala (assigned to laterobasal and superficial nuclei groups), anterior thalamus, and MTG, while cluster 3 was congruently connected to the left dlPFC. Finally, cluster 4 was congruently connected to the bilateral vmPFC, FP (assigned to area FP2), pMCC, and anterior thalamus, as well as the right hippocampus (assigned to subiculum and CA).

Specific cluster connectivity

Given the large amount of connectivity shared between the PMC clusters, we investigated what parts of the brain were more strongly connected to a given cluster than the respective three other clusters (Fig. 6). To this end, we isolated the brain regions that were selectively connected with a given cluster by contrast with all remaining clusters. For example, to delineate the connectivity specific to cluster 1, we computed an AND conjunction across the three difference maps (clusters 1 - clusters2), (cluster 1 - cluster 3), and (clusters 1 - cluster 4). This procedure removed connectivity of cluster 1 that was shared with clusters 2, 3, and 4. Please note that the ensuing maps of specific cluster connectivity survived a statistical test for significance. This is because any voxel that is deemed to reflect *specific* connectivity of a given cluster had been determined to be statistically more associated with that cluster in three separate difference analyses with the respective three other clusters.

As to MACM, cluster 1 was specifically connected to the bilateral dlPFC (at the caudal end of the middle frontal gyrus and superior frontal sulcus), IPS (assigned to hIP1 and hIP3), and SMA/MCC, as well as the right FEF, TPJ, and supramarginal gyrus (assigned to area PF). As to RSFC, cluster 1 was specifically connected to the right dlPFC (similar topography as for MACM) extending into the FEF, bilateral IPS (assigned to areas hIP1/hIP3), and right TPJ. Across MACM and RSFC, cluster 1 was congruently specifically connected to the bilateral IPS (assigned to areas hIP1/hIP3) as well as the right FEF and TPJ.

As to MACM, cluster 2 was specifically connected to the bilateral vmPFC (ventrocaudal to area FP2) and IPC (assigned to area PGp), as well as left IFG (assigned to area 45). As to RSFC, cluster 2 was specifically connected to the bilateral vmPFC (slightly extending into area FP2) and IPC (assigned to area PGp). Across MACM and RSFC, cluster 2 was congruently specifically connected to bilateral vmPFC and middle aspects of the left IPC (assigned to area PGp).

As to MACM, cluster 3 was specifically connected to the bilateral dmPFC, IPC (assigned to left area PGa and right PGp), and pMCC, as well as the left dlPFC, SPC, and posterior superior temporale sulcus. As to RSFC analyses, cluster 3 was specifically connected to the bilateral dmPFC, dlPFC, IPC (assigned to left areas PGa/PGp/PFm and right areas PGa/PGp), pMCC, MTG, TP, and cerebellum. Across MACM and RSFC, cluster 3 was congruently specifically connected to the bilateral dmPFC, pMCC, IPC (assigned to left area PGa and right area PGp), as well as the left caudal dlPFC (close to the inferior frontal junction and ventral premotor cortex).

As to MACM, cluster 4 was specifically connected to bilateral anterior thalamus and right hippocampus (assigned to CA). As to RSFC, cluster 4 was specifically connected to the bilateral hippocampus (assigned to subiculum and CA), thalamus, occipital lobe (assigned to areas 17, 18, and hOC3V), and cerebellum, as well as left amygdala (assigned to the superficial nuclei group). Across MACM and RSFC, cluster 4 was congruently specifically connected to the bilateral anterior thalamus and right hippocampus (assigned to CA).

Congruent connectivity across clusters

After the cluster-by-cluster connectivity analyses, we tested for brain regions that were congruently functionally coupled with all four PMC clusters in either the presence (MACM) or absence (RSFC) of experimental tasks (Fig. 7). In MACM, not a single brain regions was congruently connected to all four PMC clusters. In RSFC, all four PMC clusters were congruently connected to the bilateral vmPFC, FP (assigned to area FP2), dmPFC, IPC (extending into the TPJ), MTG (extending into the temporal pole on the right), posterior thalamus, hippocampus (assigned to subiculum and CA), parahippocampal gyrus, pMCC, and cerebellum. Hence, in a task-constrained cognitive set, no part of the brain was conjointly connected to all PMC clusters, whereas in a task-unconstrained cognitive set all PMC clusters were conjointly connected to a distributed network conventionally described as the “default mode network” (Buckner et al., 2008; Laird et al., 2009b).

Functional characterization

We performed quantitative functional decoding by testing for BrainMap meta-data terms associated with activation in each cluster (Fig. 8). For the sake of robustness, the description is concentrated on taxonomic associations that were significant in both forward and reverse inference analyses. Overall, the behavioral domains (BDs) and paradigm classes (PCs) of BrainMap studies activating in the four PMC clusters emphasized this associative brain region's implication in complex cognitive processes. Analogous to the connectivity profiles, the functional characterizations of the individual clusters featured a number of similarities.

All four clusters were significantly associated with explicit memory retrieval and emotion in both forward and reverse inference approaches (except for an association of emotion with cluster 1 in the reverse decoding only). Additionally, three clusters (all but cluster 4) were significantly associated with social cognition, theory-of-mind tasks, and episodic memory processing, imagination of objects and scenes, as well as cued explicit recognition across forward and reverse functional decoding. It is noteworthy that the remaining cluster 4 was by far the smallest in volume, potentially leading to lower power in the analysis of functional associations. Another set of three clusters (all but cluster 1) was associated with general cognition across forward and reverse decoding.

Only cluster 1 was associated with attentional and executive processes across forward and reverse decoding, including (deductive) reasoning, spatial processing, and perception of visual motion, as well as the Simon task, action inhibition, and pointing. Only cluster 2 was consistently associated with language and facial appraisal, only cluster 3 was consistently associated with delay discounting tasks, and only cluster 4 was consistently associated with phonological discrimination tasks.

Discussion

In this study, we used the data resources provided by BrainMap (Fox and Lancaster, 2002) to delineate the connectional and functional segregation of the posterior medial cortex (PMC). Regional differences in whole-brain coactivation patterns suggested a subdifferentiation of the PMC into four distinct functional modules. The coactivation-derived clusters corresponded to the PrC, ventral and dorsal posterior cingulate cortex (vPCC/dPCC), as well as retrosplenial cortex (RSC). These four clusters were subsequently characterized by task-dependent and task-independent functional connectivity mapping and forward/reverse inference on associated functions. Although the clusters shared common connectional and functional properties, results of our analyses suggest that cluster 1 (PrC) might be more related to initiating shifts of attentional focus, clusters 2 and 3 (vPCC and dPCC) are more related to processing predominantly object- and space-related facets, respectively, and cluster 4 (RSC) mediates shifts between focusing on current sensory environment and assuming a (decoupled) world perspectives. This four-fold set of general neural processes might underlie the frequent involvement of the PMC across the boundaries of classical cognitive domains. In this section, we will first focus on the strongest whole-brain connections and exclusive functional associations of each cluster and subsequently discuss the overall connectional and functional profiles in a dedicated paragraph (“Functional integration at task and rest”).

Cluster1: Precuneus related to attentional shifting

Cluster 1 (medial portion of BA 7) is the only connectivity-derived region of our PMC VOI that is neuroanatomically situated in the PrC (i.e., parietal lobe proper) rather than PCC or RSC (i.e., cingulate cortex). This is relevant insofar as the posterior cingulate cortex (clusters 2 and 3) is at times unfortunately labeled “precuneus” in the neuroimaging literature (cf. Margulies et al., 2009). Cluster 1 in the PMC was *selectively* connected (i.e., more strongly than any of the three other clusters) to the right frontal eye field (FEF),

bilateral intraparietal sulcus (IPS), and *right* temporo-parietal junction, congruently across task-related (MACM) and task-unrelated (RSFC) analyses. This connectivity pattern of cluster 1 corroborates that the PrC is perhaps *not* part of the default mode network (DMN; Buckner et al., 2008; Margulies et al., 2009; Parvizi et al., 2006; Zhang and Li, 2012). In line with this idea, DMN-typical blood flow decreases during most externally structured tasks (Buckner et al., 2008; Bzdok et al., 2013b; Gusnard and Raichle, 2001; Laird et al., 2009b) were observed in the vPCC and RSC but not in PrC as indicated by arterial spin labeling imaging (Pfefferbaum et al., 2011). Notably, a recent RSFC-based parcellation study of the human PrC showed that its ventral, but not dorsal, clusters exhibited connectivity with the DMN (Zhang and Li, 2012).

Cluster 1 and the specifically connected right FEF and bilateral IPS (across MACM and RSFC) form a network known to be monosynaptically connected from axonal tracing studies in monkeys (Cavada and Goldman-Rakic, 1989b; Parvizi et al., 2006; Schall et al., 1995) and to be closely related to internally or externally provoked spatial attentional modulation (Corbetta et al., 2008; Gitelman et al., 1999; Mesulam, 1981). This is in line with the present results as cluster 1 was exclusively functionally associated with spatial reflection, pointing, perception of visual motion, and spatial conflict resolution in the Simon task across forward and reverse functional decoding. More specifically, this PMC region's connectional and functional properties agree with an implication in the dorsomedial motor stream (Rizzolatti and Matelli, 2003). Overtly, electrical stimulation in this area in monkeys evoked saccade-like eye movements (Thier and Andersen, 1998), while visually-guided saccades entailed single-cell activity in that area (Ferraina et al., 1997). Covertly, triggered attentional shifts in the absence of eye movements elicited increased neural activity in the PrC, FEF, and IPS during a stimulus discrimination fMRI task in humans (Gitelman et al., 1999). Additionally, this brain region increased activity during imagined (but not executed) motor movements of joysticks (Stephan et al., 1995) and fingers (Gerardin et al., 2000), thus relating it to the notion of a visumotor cycles. Internally and externally motivated attentional reallocation is also associated with the right temporo-parietal junction (Bzdok et al., 2013b; Corbetta et al., 2008; Decety and Lamm, 2007; Koster-Hale and Saxe, 2013; Langner et al., 2012) that is specifically connected to cluster 1 in the present study (Table 1). Concurrently, the right temporo-parietal junction is the most frequent lesion focus leading to hemi-neglect (Corbetta et al., 2000; Vallar and Perani, 1987), that is, failure to orient attention to the contra-lesional side. The right temporo-parietal junction lesions thus entail loss of awareness of both the self and the environment (Blumenfeld, 2002). In line with present and previous findings, we are enticed to speculate that cluster 1 is implicated in the internally or externally triggered, overt or covert allocation of attentional resources to internal or external information.

Cluster2: Ventral posterior cingulate cortex related to objects

Cluster 2, located in the vPCC (ventral aspects of BA 23 and 31), was specifically connected to the bilateral ventromedial prefrontal cortex (vmPFC) and aspects of the left IPC, congruently across task-related (MACM) and task-unrelated (RSFC) brain activity. While the vPCC and vmPFC are monosynaptically connected in monkey tracing studies (Carmichael and Price, 1995), the existence of definite IPC homologues in monkeys is a

matter of debate (Caspers et al., 2011; Mars et al., 2013; Seghier, 2013). It is important to appreciate that a ventral-dorsal dissociation of the PCC has been advocated based on connectional arguments in monkeys (Cavada and Goldman-Rakic, 1989a; Vogt and Barbas, 1988; Vogt and Pandya, 1987) as well as on immunohistochemistry, receptor architecture, and functional implications in humans (Palomero-Gallagher et al., 2009; Vogt et al., 2006). In line with these experimental findings, the present coactivation-based PMC parcellation and an earlier RSFC-based PMC parcellation (Cauda et al., 2010) in humans agreed on dividing the PCC into a ventral and a dorsal compartment. The present PCC subdivision was primarily driven by a congruent cluster-specific connectivity to the vmPFC (vPCC) versus dmPFC (dPCC).

Qualitative and quantitative reviews portrayed the vmPFC as more related to evaluation and reward processing when juxtaposed with the dmPFC (Bzdok et al., 2012b; Bzdok et al., 2013a; Gläscher et al., 2012; Kringelbach and Rolls, 2004). Matching this view, only cluster 2 was congruently coupled (across MACM and RSFC) with the amygdala (involved in significance evaluation) and the nucleus accumbens (involved in reward evaluation) as well as exclusively functionally associated with facial appraisal. Similarly, the human vPCC was the only PMC region connected to the laterobasal (rather than centromedial or superficial) nuclei group of the amygdala (Bzdok et al., 2012a), which is an amygdalar subregion probably devoted to continuously scanning environmental input for biological significance (Adolphs, 2010; Aggleton et al., 1980; Bzdok et al., 2011; Ghods-Sharifi et al., 2009; LeDoux, 2007). Consistently, single-cell recordings in the monkey PCC demonstrated this brain region's sensitivity to subjective target utility (McCoy and Platt, 2005) and integration across individual outcomes in decision making (Pearson et al., 2009). Further single-cell recordings in monkeys showed that in PCC activity predicted behavior in upcoming trials in a reward outcome evaluation task, while microstimulation in this region impeded learning of choice-reward associations (Hayden et al., 2008). This entices to speculate that the human vPCC mediates self-relevance assessment, potentially extending to the hierarchically higher processes self-monitoring and self-reflection (Bzdok et al., 2013a; Johnson et al., 2002; Kircher et al., 2001; Krienen et al., 2010; Vogt, 2005). More specifically, such a predominantly *evaluative*, rather than genuinely *emotional*, functional role of the vPCC is also corroborated by (i) the known lack of autonomic projections to subcortical autonomic motor nuclei, supported by the present results, (ii) absent autonomic changes during electrical stimulation, and (iii) reports of activation increases during appraisal of both emotional and non-emotional stimuli in neuroimaging studies (Baleydier and Mauguire, 1980; Vogt et al., 2003; Vogt et al., 2006).

A role in the evaluation of stimulus characteristics, as opposed to space characteristics, would fit with the well-known relation of the vPCC to the ventral visual stream - the “what” system for object processing (Ungerleider and Haxby, 1994; Ungerleider and Mishkin, 1982; Vogt et al., 2006), contrary to the dPCC's conceivable relation to the dorsal “where” system (cf. below). Indeed, knowledge retrieval of landmarks (i.e., stimulus characteristics) versus routes (i.e., spatial characteristics) increased neural activity in the more ventral versus more dorsal PCC, respectively (Maguire et al., 1997). Interestingly, hyperconnectivity of the vPCC was reported in autism (Lynch et al., 2013), a developmental spectrum disorder

characterized by overly meticulous attention to object details and seemingly treating social stimuli as non-social objects (Klin et al., 2002; Pelphrey et al., 2002). Such evaluation processes of stimulus characteristics might resort to the retrieval of associated semantic categories, as suggested by two present findings. First, the vPCC was exclusively functionally associated with language processing across functional decoding modalities. Second, the vPCC was specifically connected to aspects of the left middle IPC, the most robust correlate of the neural semantic system (cf. Binder et al., 2009; Déjerine, 1891; Hensel et al., in press; Seghier, 2013). In line with present and previous findings, we are enticed to speculate that cluster 2 in the PMC VOI is implicated in predominantly evaluating object features, as opposed to space features, in perceived or imagined visual stimuli, potentially informed by semantic concepts.

Cluster3: Dorsal posterior cingulate cortex related to space

Cluster 3, located in the dPCC (dorsal aspects of BA 23 and 31), was specifically connected to the bilateral dorsomedial prefrontal cortex (dmPFC), posterior midcingulate cortex (pmCC), and inferior parietal cortex (IPC) as well as to the left dorsolateral prefrontal cortex (dlPFC), congruently across MACM and RSFC analyses. Also in monkeys, the dPCC was found to be connected to the dmPFC (Cavada and Goldman-Rakic, 1989b) and posterior parietal cortex (Cavada and Goldman-Rakic, 1989a; Vogt and Pandya, 1987) in axonal tracing studies and to the pmCC and dlPFC in a RSFC study (Margulies et al., 2009). Notably, qualitative and quantitative reviews portrayed the dmPFC as more related to mental-scene creation and abstraction, as compared to the vmPFC (Bzdok et al., 2012b; Bzdok et al., 2013a; Eickhoff et al., in press; Frith and Frith, 2003; Gallagher and Frith, 2003; Ochsner, 2008).

This view is in line with the well-known integration of the dPCC's in the dorsal visual stream - the “where” system for spatial processing (Ungerleider and Haxby, 1994; Ungerleider and Mishkin, 1982; Vogt et al., 2006), in contrast to vPCC's relation to the ventral “what” system (cf. above). Receiving support from neuroimaging in humans, dPCC activity increased during self-paced navigation through realistic virtual environments (Maguire et al., 1998; Maguire et al., 1997), visual feedback of moving hands (Inoue et al., 1998), and the prediction of self-generated actions (Blakemore et al., 1998). Congruently, the dPCC here exhibited specific connectivity to the pmCC, a cingulate motor region implicated in skeletomotor orientation and movement initiation (Morecraft and Van Hoesen, 1992; Shima et al., 1991; Vogt et al., 2003). Additionally, direct electrical stimulation of the dPCC in presurgical epileptic humans evoked complex proprioceptive sensations (Richer et al., 1993).

The dPCC's functional spectrum probably extends to highly abstract facets of processing navigation. This was, for instance, suggested by dPCC gray-matter volume correlating with meta-cognitive capacity in a spatial memory task (McCurdy et al., 2013). Moreover, the dPCC is unlikely to instantiate genuinely emotional computations (Baleydier and Mauguire, 1980; Vogt et al., 2003; Vogt and Laureys, 2005; Vogt et al., 2006), analogous to the vPCC, considering (i) the sheer abundance of evidence for the dPCC's role in spatial navigation and (ii) its specific connectivity to cognitive rather than emotional brain regions,

including the (here observed) dlPFC and IPC. In line with present and previous findings, we are enticed to speculate that cluster 3 in the PMC VOI is implicated in overt and covert navigation of the self and body in real or imagined spatial environments.

Cluster4: Retrosplenial and adjacent cortex related to perspective frames

Cluster 4 contains parts of the retrosplenial cortex (mainly BA 30) and the PCC area BA 23, i.e., its ventroposterior part. The largest part of BA 23, however, is covered by clusters 2 and 3. The major part of cluster 4 is found in a topographic position that is best comparable to subarea 23v in macaque monkeys (Kobayashi and Amaral, 2000), which is the most caudoventral part of the cingulate gyrus. Note that the present somewhat liberal RSC cluster might correspond very well to what is frequently called “retrosplenial complex/cortex” in the neuroimaging literature (Bar and Aminoff, 2003; Yomogida et al., 2014). Cluster 4 was prominently connected to the right hippocampus and bilateral anterior thalamus, congruently across MACM and RSFC analyses. Also in monkeys, the retrosplenial cortex featured particularly strong axonal connections with these two brain regions (Kobayashi and Amaral, 2003, 2007; Parvizi et al., 2006; Vogt et al., 1987).

Functionally, the RSC is frequently noted to be involved in moving across both time, e.g. autobiographical memory, and space, e.g. navigation in ambient environment (Spreng et al., 2009; Vann et al., 2009). Regarding memory processing, lesions in the RSC, as compared to other PMC regions, is most consistently associated with anterograde and retrograde memory impairments of different types of sensory information in rabbits (Gabriel and Talk, 2001) and humans (Rudge and Warrington, 1991; Valenstein et al., 1987). Regarding spatial processing, lesions in the RSC are consistently associated with impaired processing of spatial information and recognition of novel locations in rodents (Aggleton and Vann, 2004; Harker and Whishaw, 2004) as well as a lost sense of direction and location in humans (Aguirre and D'Esposito, 1999; Takahashi et al., 1997). Additionally, lesions of the anterior thalamic nuclei, which we here found to be connected to the RSC, impaired object-in-place recall in monkeys (Parker and Gaffan, 1997). In sum, the observed connectivity patterns and functional associations (with explicit memory retrieval) corroborate earlier studies in the RSC's close relationship to handling both memory and spatial information. From a hierarchical perspective on cognitive processing, the RSC appears to predominantly subserve the *binding* and *integration* of memories and places, rather than processing any of these two content categories per se (cf. Aguirre and D'Esposito, 1999; Epstein, 2008; Vann and Aggleton, 2002).

As memory and spatial processes constitute two diverging cognitive classes, this dual relationship of cluster 4 can thus be read as indicating a more domain-overarching functional role. More specifically, current findings and earlier lesion reports can be parsimoniously reconciled by the previously proposed notion that the RSC mediates between the organism's egocentric (i.e., focused on sensory input) and allocentric (i.e., focused on world knowledge) perspective frames (Burgess, 2008; Epstein, 2008; Valiquette and McNamara, 2007). Indeed, RSC-lesioned humans cannot draw *envisioned* spaces of familiar environments (i.e., translation from ego- to allo-centric perspective) and are impaired at inferring their body orientation in the *actual* environment from maps (i.e., translation from allo- to ego-centric

perspective) (Maguire, 2001; Yoder et al., 2011). This might also explain why neural activity in the animal RSC was not tonically maintained during spatial navigation in familiar environments (Burgess et al., 2001; Byrne et al., 2007; Vann et al., 2009). Concurrently, neural activity in the human RSC (but no other PMC region) correlated with individuals' perspective-taking capacity (Meyer and Lieberman, 2012).

Assuming the human RSFC to flip between ego and world perspectives, the connections, observed in the present study, to the thalamus could furnish information on the sensory viewpoint offset, whereas the observed connections to the hippocampus might furnish memory and spatial content (Byrne et al., 2007; Maguire et al., 1997; Scoville and Milner, 1957; von Bechterew, 1900). In line with present and previous findings, we are enticed to speculate that cluster 4 in the PMC VOI is implicated in mediating between organism-centered (i.e., egocentric or from current view) and world-centered (i.e., allocentric or from a bird's eye view) perspective frames, which is a frequent feature of both processing memory and spatial scenes.

Relation to recent studies on the PMC

A previous topographical parcellation of the PMC based on RSFC by Cauda and colleagues (2010) closely relates to the here obtained PMC clusters. This study, however, additionally subdivided the precuneus into a rostradorsal and a caudoventral cluster, while we additionally subdivided the ventral PMC into vPCC and RSC. Another CBP study based on RSFC (Zhang and Li, 2012) was restricted to the precuneus without considering the cortical regions of the here revealed vPCC, dPCC, and RSC clusters. A diffusion tensor imaging (DTI) based parcellation of the PMC also identified a more ventral and a more dorsal cluster in the PCC/RSC region, but further subdivided the precuneus into three parts (Zhang et al., 2014). Additionally, a VOI in the posterior cingulate cortex drawn from the Harvard-Oxford atlas was parcellated using independent component analysis of the VOI voxels' RSFC (Leech et al., 2012). Only the most caudal of the ensuing clusters coincided with the present PMC VOI. This previous cluster and the corresponding present dPCC cluster agree in strong functional connectivity to the dmPFC and bilateral IPC.

The regional connectivity differences of the PMC in humans and macaque monkeys were compared using RSFC (Margulies et al., 2009). Based on strong connectivity to the vmPFC, dmPFC, and medial temporal region, the vPCC, dPCC, and RSC were argued to belong to a limbic component of the PMC in humans and monkeys. Based on strong connectivity to the dlPFC and IPC, the precuneus, in turn, could belong to a cognitive part of the PMC in both species. Our connectivity results concur with this across-species connectivity study. Importantly, however, the present results deemphasize an emotion-cognition schism (cf. Pessoa, 2008; Van Overwalle, 2011) in the functional subspecialization of the PMC.

Taken together, the topography of the present PMC clusters roughly replicates previous parcellations of hand-drawn and atlas-provided VOIs using structural and functional connectivity analyses. The present clusters' connectivity patterns agree with previous connectivity findings from humans and monkeys. Extending previous PMC investigations, we provide a multi-dimensional perspective on the PMC by integration of i) a

neuroanatomically meaningful PMC segregation, ii) a cluster characterization by complementary connectivity measures acknowledging opposing brain states, as well as iii) a bimodal functional decoding thereof.

Functional integration at task and rest

We also tested what parts of the brain were congruently connected to *all of the four derived clusters* of the PMC VOI. In the MACM analyses, reflecting functional coupling between brain regions during experimentally imposed cognitive sets, no brain region outside the PMC was congruently linked to all four clusters. In the RSFC analyses, reflecting functional coupling between brain regions during mental activity without externally imposed constraints, all four clusters were congruently linked to a network comprising the bilateral vmPFC, frontal pole (assigned to area FP2), dmPFC, IPC (extending into the TPJ), middle temporal gyrus (extending into the temporal pole on the right), posterior thalamus, hippocampus (assigned to subiculum and CA), parahippocampal gyrus, pMCC, and cerebellum. This set of brain regions is known to form a cohesive functional unit, the so-called DMN (Gusnard et al., 2001; Laird et al., 2009b; Schilbach et al., 2012; Spreng et al., 2009). Hence, the PMC regions did not engage any common brain region or network during task-related information processing, while they conjointly engaged a well-characterized network during task-unrelated information processing. These findings also emphasize that a dichotomic brain segregation into clear-cut “task-positive” and “task-negative” brain regions probably constitutes an undue oversimplification (Bzdok et al., 2013b; Eickhoff et al., in press; Kelly et al., 2012; Murphy et al., 2009). That is because the PrC exhibited both “task-negative” properties, for example, in its functional coupling with DMN regions at rest in the present study, as well as “task-positive” properties, for example, in earlier studies on regional cerebral blood flow in humans measured by arterial spin labeling (Pfefferbaum et al., 2011) and functional connectivity patterns in monkeys (Margulies et al., 2009). Nevertheless, we are tempted to speculate that, during task engagement (MACM), the four PMC clusters do probably not collaborate functionally towards a shared computational goal, whereas, during rest (RSFC), all clusters might perhaps closely functionally integrated in a network corresponding to the DMN.

In fact, the DMN is often proposed to be dedicated to continuous autobiographical memory retrieval, environmental assessment, emotion appraisal, and reward contingency evaluation when letting the mind go. Constantly tracking and predicting changes in a variable environment is believed to then shape the internal milieu and upcoming external behavior adaptively (Binder et al., 1999; Bzdok et al., 2013b; Hayden et al., 2008; James, 1890; Schacter et al., 2007; Schilbach et al., 2008). This frequent contention in the literature is supported by the present results as *all four clusters* were functionally associated with memory retrieval and emotion processing and different sets of three clusters were associated with general cognition, imagination of objects and scenes, episodic memory recall, as well as social cognition and theory-of-mind tasks. In sum, parts of the DMN might subserve a variety of mental processes when collaborating with other more domain-specific brain regions in a task-focused mindset (cf. Seghier, 2013), while the DMN as a cohesive functional unit subserves a small set of mental operations related to emotion, reward, and memories in a task-unfocused mindset.

Such mind-wandering at rest might be subserved by different neural computations implemented in the four components of the PMC established in the present study. Note that 'mind-wandering' is used here in the broad sense of cognitive processes that are not controlled by a certain task, which makes no judgment about the content of these thought processes. Integrating the above cluster-wise interpretations, mind-wandering might be instantiated by internally navigating the self in mapped hypothetical, present, future, or past spaces (dPCC potentially mediating spatial scene elaboration, RSC potentially mediating the translation between ego and world oriented reference frames) to allow detecting behaviorally relevant features in those envisioned scenes (vPCC potentially mediating self-relevance evaluation) by shifting the attentional focus between various feature and aspect contemplations (PrC potentially mediating the covert reallocation of attentional resources between different internal representations). Note that this does not necessarily imply functional PMC segregation by exclusively self- or exclusively other-related components because the probably domain-global PMC cluster functions could subserve both self- and other-related processes. Ultimately, if these speculations hold some truth in them, the PMC's conceivable key role in the continuous environmental tracking in a generative, integrative process might explain both its highest energy consumption in the brain and its intimate coupling with conscious awareness.

Limitations

The present methodological approach aimed at the neurobiological characterization of the human PMC involves noteworthy drawbacks. For mapping task-based coactivations (i.e. MACM) of our seed region, we used the neuroimaging activation coordinates stored in the BrainMap database (Fox and Lancaster, 2002; Laird et al., 2011a). It currently contains the paper-published coordinates of approximately 12,000 neuroimaging experiments and thus covers approximately 25% of the entire neuroimaging literature. Compared to other neuroimaging databases, BrainMap is most extensive in the number of hosted experiments and in the richness of meta-data provided with these (cf. Derrfuss and Mar, 2009). However, lacking coverage of the entire literature conceivably entails that certain paradigms/tasks are over- or underrepresented in the here used database. That is, the present MACM analyses could have resulted in connectivity estimates that might be partly influenced by selection bias.

MACM is based on coordinate-based meta-analysis (Eickhoff et al., 2012; Radua and Mataix-Cols, 2009; Wager et al., 2007). This has a well-recognized alternative, namely, image-based meta-analysis (Schilbach et al., 2008). Drawing on the comprehensive statistical images acknowledges the complete 3D activation shapes of each neuroimaging experiment. Yet, image-based meta-analysis necessitates other investigators' collaborative effort, which often entails small experiment samples (Eickhoff and Bzdok, 2012). Coordinate-based meta-analysis, on the other hand, can summarize complete literature bodies and provides very similar activation convergence results to classical neuroimaging studies on corresponding cognitive phenomena (Turkeltaub et al., 2002). In light of routinely applied smoothing procedures, imperfect warping of individual brains to standard reference spaces, and interindividual neuroanatomical differences focus on activation peaks, rather

than activation shapes, constraints meta-analytical investigations to the essence of BOLD signal information.

Acknowledgments

This study was supported by the Deutsche Forschungsgemeinschaft (DFG, EI 816/4-1 to S.B.E. and L.A. 3071/3-1 to R.L. and S.B.E.; EI 816/6-1 to S.B.E. and D.B.), the National Institute of Mental Health (R01-MH074457 to A.R.L., P.T.F., and S.B.E.), the Helmholtz Initiative on Systems Biology (Human Brain Model to K.Z. and S.B.E.), and the German National Academic Foundation (D.B.).

References

- Adolphs R. What does the amygdala contribute to social cognition? *Ann N Y Acad Sci.* 2010; 1191:42–61. [PubMed: 20392275]
- Aggleton JP, Burton MJ, Passingham RE. Cortical and subcortical afferents to the amygdala of the rhesus monkey (*Macaca mulatta*). *Brain Res.* 1980; 190:347–368. [PubMed: 6768425]
- Aggleton JP, Vann SD. Testing the importance of the retrosplenial navigation system: lesion size but not strain matters: a reply to Harker and Whishaw. *Neurosci Biobehav Rev.* 2004; 28:525–531. [PubMed: 15465139]
- Aguirre GK, D'Esposito M. Topographical disorientation: a synthesis and taxonomy. *Brain.* 1999; 122(Pt 9):1613–1628. [PubMed: 10468502]
- Amunts K, Kedo O, Kindler M, Pieperhoff P, Mohlberg H, Shah NJ, Habel U, Schneider F, Zilles K. Cytoarchitectonic mapping of the human amygdala, hippocampal region and entorhinal cortex: intersubject variability and probability maps. *Anat Embryol (Berl).* 2005; 210:343–352. [PubMed: 16208455]
- Amunts K, Malikovic A, Mohlberg H, Schormann T, Zilles K. Brodmann's areas 17 and 18 brought into stereotaxic space—where and how variable? *Neuroimage.* 2000; 11:66–84. [PubMed: 10686118]
- Amunts K, Schleicher A, Burgel U, Mohlberg H, Uylings HB, Zilles K. Broca's region revisited: cytoarchitecture and intersubject variability. *J Comp Neurol.* 1999; 412:319–341. [PubMed: 10441759]
- Ashburner J, Friston KJ. Unified segmentation. *Neuroimage.* 2005; 26:839–851. [PubMed: 15955494]
- Baleydier C, Mauguier F. The duality of the cingulate gyrus in monkey. *Neuroanatomical study and functional hypothesis.* *Brain.* 1980; 103:525–554. [PubMed: 6774795]
- Bar M, Aminoff E. Cortical analysis of visual context. *Neuron.* 2003; 38:347–358. [PubMed: 12718867]
- Berger H. On the electroencephalogram of man: third report. *Electroenceph Clin Neurophysio.* 1931; (Supplement No. 28):95–132.
- Binder JR, Desai RH, Graves WW, Conant LL. Where is the semantic system? A critical review and meta-analysis of 120 functional neuroimaging studies. *Cereb Cortex.* 2009; 19:2767–2796. [PubMed: 19329570]
- Binder JR, Frost JA, Hammeke TA, Bellgowan PS, Rao SM, Cox RW. Conceptual processing during the conscious resting state: a functional MRI study. *J Cogn Neurosci.* 1999; 11:80–93. [PubMed: 9950716]
- Biswal B, Yetkin FZ, Haughton VM, Hyde JS. Functional connectivity in the motor cortex of resting human brain using echo-planar MRI. *Magn Reson Med.* 1995; 34:537–541. [PubMed: 8524021]
- Blakemore SJ, Rees G, Frith CD. How do we predict the consequences of our actions? A functional imaging study. *Neuropsychologia.* 1998; 36:521–529. [PubMed: 9705062]
- Bludau S, Eickhoff SB, Mohlberg H, Caspers S, Laird AR, Fox PT, Schleicher A, Zilles K, Amunts K. Cytoarchitecture, probability maps and functions of the human frontal pole. *Neuroimage.* 2013
- Blumenfeld, H. *Neuroanatomy through Clinical Cases.* Sinauer Associates; Sunderland, MA, USA: 2002.
- Buckner RL, Andrews-Hanna JR, Schacter DL. The brain's default network: anatomy, function, and relevance to disease. *Ann N Y Acad Sci.* 2008; 1124:1–38. [PubMed: 18400922]

- Burgess N. Spatial cognition and the brain. *Ann N Y Acad Sci.* 2008; 1124:77–97. [PubMed: 18400925]
- Burgess N, Becker S, King JA, O'Keefe J. Memory for events and their spatial context: models and experiments. *Philos Trans R Soc Lond B Biol Sci.* 2001; 356:1493–1503. [PubMed: 11571039]
- Byrne P, Becker S, Burgess N. Remembering the past and imagining the future: a neural model of spatial memory and imagery. *Psychol Rev.* 2007; 114:340–375. [PubMed: 17500630]
- Bzdok D, Laird A, Zilles K, Fox PT, Eickhoff SB. An investigation of the structural, connectional and functional sub-specialization in the human amygdala. *Hum Brain Mapp.* 2012a in press.
- Bzdok D, Langner R, Caspers S, Kurth F, Habel U, Zilles K, Laird A, Eickhoff SB. ALE meta-analysis on facial judgments of trustworthiness and attractiveness. *Brain Struct Funct.* 2011; 215:209–223. [PubMed: 20978908]
- Bzdok D, Langner R, Hoffstaedter F, Turetsky BI, Zilles K, Eickhoff SB. The modular neuroarchitecture of social judgments on faces. *Cereb Cortex.* 2012b; 22:951–961. [PubMed: 21725038]
- Bzdok D, Langner R, Schilbach L, Engemann D, Laird AR, Fox PT, Eickhoff SB. Segregation of the human medial prefrontal cortex in social cognition. *Front Hum Neurosci.* 2013a
- Bzdok D, Langner R, Schilbach L, Jakobs O, Roski C, Caspers S, Laird A, Fox PT, Zilles K, Eickhoff SB. Characterization of the temporo-parietal junction by combining data-driven parcellation, complementary connectivity analyses, and functional decoding. *Neuroimage.* 2013b in press.
- Carmichael ST, Price JL. Limbic connections of the orbital and medial prefrontal cortex in macaque monkeys. *J Comp Neurol.* 1995; 363:615–641. [PubMed: 8847421]
- Caspers S, Eickhoff SB, Rick T, von Kapri A, Kuhlen T, Huang R, Shah NJ, Zilles K. Probabilistic fibre tract analysis of cytoarchitectonically defined human inferior parietal lobule areas reveals similarities to macaques. *Neuroimage.* 2011; 58:362–380. [PubMed: 21718787]
- Caspers S, Geyer S, Schleicher A, Mohlberg H, Amunts K, Zilles K. The human inferior parietal cortex: cytoarchitectonic parcellation and interindividual variability. *Neuroimage.* 2006; 33:430–448. [PubMed: 16949304]
- Cauda F, Cavanna AE, D'Agata F, Sacco K, Duca S, Geminiani GC. Functional connectivity and coactivation of the nucleus accumbens: a combined functional connectivity and structure-based meta-analysis. *J Cogn Neurosci.* 2011; 23:2864–2877. [PubMed: 21265603]
- Cauda F, Geminiani G, D'Agata F, Sacco K, Duca S, Bagshaw AP, Cavanna AE. Functional connectivity of the posteromedial cortex. *PLoS One.* 2010; 5
- Cavada C, Goldman-Rakic PS. Posterior parietal cortex in rhesus monkey: I. Parcellation of areas based on distinctive limbic and sensory corticocortical connections. *J Comp Neurol.* 1989a; 287:393–421. [PubMed: 2477405]
- Cavada C, Goldman-Rakic PS. Posterior parietal cortex in rhesus monkey: II. Evidence for segregated corticocortical networks linking sensory and limbic areas with the frontal lobe. *J Comp Neurol.* 1989b; 287:422–445. [PubMed: 2477406]
- Cavanna AE, Trimble MR. The precuneus: a review of its functional anatomy and behavioural correlates. *Brain.* 2006; 129:564–583. [PubMed: 16399806]
- Chang LJ, Yarkoni T, Khaw MW, Sanfey AG. Decoding the role of the insula in human cognition: functional parcellation and large-scale reverse inference. *Cereb Cortex.* 2013; 23:739–749. [PubMed: 22437053]
- Chang SE, Kenney MK, Loucks TM, Poletto CJ, Ludlow CL. Common neural substrates support speech and non-speech vocal tract gestures. *Neuroimage.* 2009; 47:314–325. [PubMed: 19327400]
- Cieslik EC, Zilles K, Caspers S, Roski C, Kellermann TS, Jakobs O, Langner R, Laird AR, Fox PT, Eickhoff SB. Is There “One” DLPFC in Cognitive Action Control? Evidence for Heterogeneity From Co-Activation-Based Parcellation. *Cereb Cortex.* 2012
- Clos M, Amunts K, Laird AR, Fox PT, Eickhoff SB. Tackling the multifunctional nature of Broca's region meta-analytically: Co-activation-based parcellation of area 44. *Neuroimage.* 2013; 83C: 174–188. [PubMed: 23791915]
- Corbetta M, Kincade JM, Ollinger JM, McAvoy MP, Shulman GL. Voluntary orienting is dissociated from target detection in human posterior parietal cortex. *Nat Neurosci.* 2000; 3:292–297. [PubMed: 10700263]

- Corbetta M, Patel G, Shulman GL. The reorienting system of the human brain: from environment to theory of mind. *Neuron*. 2008; 58:306–324. [PubMed: 18466742]
- Couch, D.; Dawson, G.; Fischer, KW. *Human Behavior, Learning, and the Developing Brain: Atypical Development*. The Guilford Press; New York: 2007.
- Dastjerdi M, Foster BL, Nasrullah S, Rauschecker AM, Dougherty RF, Townsend JD, Chang C, Greicius MD, Menon V, Kennedy DP, Parvizi J. Differential electrophysiological response during rest, self-referential, and non-self-referential tasks in human posteromedial cortex. *Proc Natl Acad Sci U S A*. 2011; 108:3023–3028. [PubMed: 21282630]
- Decety J, Lamm C. The role of the right temporoparietal junction in social interaction: how low-level computational processes contribute to meta-cognition. *Neuroscientist*. 2007; 13:580–593. [PubMed: 17911216]
- Déjerine J. Sur un cas de cécité verbale avec agraphie, suivi d'autopsie. *Mémoires de la Société de Biologie*. 1891; 3:197–201.
- Derrfuss J, Mar RA. Lost in localization: The need for a universal coordinate database. *Neuroimage*. 2009; 48:1–7. [PubMed: 19457374]
- Eickhoff SB; Bzdok, D. Meta-analyses in basic and clinical neuroscience: State of the art and perspective. In: Ulmer, S.; Jansen, O., editors. *fMRI – Basics and Clinical Applications*. Springer; Heidelberg: 2012.
- Eickhoff SB, Bzdok D, Laird AR, Kurth F, Fox PT. Activation likelihood estimation meta-analysis revisited. *Neuroimage*. 2012; 59:2349–2361. [PubMed: 21963913]
- Eickhoff SB, Bzdok D, Laird AR, Roski C, Caspers S, Zilles K, Fox PT. Co-activation patterns distinguish cortical modules, their connectivity and functional differentiation. *Neuroimage*. 2011; 57:938–949. [PubMed: 21609770]
- Eickhoff SB, Laird AR, Fox PT, Bzdok D, Hensel L. Functional segregation of the human dorsomedial prefrontal cortex. *Cereb Cortex*. in press.
- Eickhoff SB, Laird AR, Grefkes C, Wang LE, Zilles K, Fox PT. Coordinate-Based Activation Likelihood Estimation Meta-Analysis of Neuroimaging Data: A Random-Effects Approach Based on Empirical Estimates of Spatial Uncertainty. *Hum Brain Mapp*. 2009; 30:2907–2926. [PubMed: 19172646]
- Epstein RA. Parahippocampal and retrosplenial contributions to human spatial navigation. *Trends Cogn Sci*. 2008; 12:388–396. [PubMed: 18760955]
- Ferraina S, Johnson PB, Garasto MR, Battaglia-Mayer A, Ercolani L, Bianchi L, Lacquaniti F, Caminiti R. Combination of hand and gaze signals during reaching: activity in parietal area 7 m of the monkey. *J Neurophysiol*. 1997; 77:1034–1038. [PubMed: 9065868]
- Fiset P, Paus T, Daloz T, Plourde G, Meuret P, Bonhomme V, Hajj-Ali N, Backman SB, Evans AC. Brain mechanisms of propofol-induced loss of consciousness in humans: a positron emission tomographic study. *J Neurosci*. 1999; 19:5506–5513. [PubMed: 10377359]
- Flechsig, P. *Anatomie des menschlichen Gehirns und Rückenmarks auf myelogenetisch Grundlage*. Thieme; Leipzig: 1920.
- Forgy EW. Cluster analysis of multivariate data: efficiency versus interpretability of classifications. *Biometrics*. 1965; 21:768–769.
- Fox DF, Raichle ME. Spontaneous fluctuations in brain activity observed with functional magnetic resonance imaging. *Nat Rev Neurosci*. 2007; 8:700–711. [PubMed: 17704812]
- Fox MD, Zhang D, Snyder AZ, Raichle ME. The global signal and observed anticorrelated resting state brain networks. *J Neurophysiol*. 2009; 101:3270–3283. [PubMed: 19339462]
- Fox PT, Laird AR, Fox SP, Fox PM, Uecker AM, Crank M, Koenig SF, Lancaster JL. BrainMap taxonomy of experimental design: Description and evaluation. *Hum Brain Mapp*. 2005; 25:185–198. [PubMed: 15846810]
- Fox PT, Lancaster JL. Opinion: Mapping context and content: the BrainMap model. *Nat Rev Neurosci*. 2002; 3:319–321. [PubMed: 11967563]
- Frith U, Frith CD. Development and neurophysiology of mentalizing. *Philos Trans R Soc Lond B Biol Sci*. 2003; 358:459–473. [PubMed: 12689373]
- Gabriel, M.; Talk, AC. A tale of two paradigms: lessons learned from parallel studies of discriminative instrumental learning and classical eyeblink conditioning. In: Steinmetz, JA.;

- Gluck, M.; Soloman, RR., editors. *Model Systems and the Neurobiology of Associative Learning*. Erlbaum, Erlbaum; Mahwah, New Jersey: 2001. p. 149-185.
- Gallagher HL, Frith CD. Functional imaging of 'theory of mind'. *Trends Cogn Sci*. 2003; 7:77–83. [PubMed: 12584026]
- Gerardin E, Sirigu A, Lehericy S, Poline JB, Gaymard B, Marsault C, Agid Y, Le Bihan D. Partially overlapping neural networks for real and imagined hand movements. *Cereb Cortex*. 2000; 10:1093–1104. [PubMed: 11053230]
- Ghods-Sharifi S, St Onge JR, Floresco SB. Fundamental contribution by the basolateral amygdala to different forms of decision making. *J Neurosci*. 2009; 29:5251–5259. [PubMed: 19386921]
- Gitelman DR, Nobre AC, Parrish TB, LaBar KS, Kim YH, Meyer JR, Mesulam M. A large-scale distributed network for covert spatial attention: further anatomical delineation based on stringent behavioural and cognitive controls. *Brain*. 1999; 122(Pt 6):1093–1106. [PubMed: 10356062]
- Gläscher J, Adolphs R, Damasio H, Bechara A, Rudrauf D, Calamia M, Paul LK, Tranel D. Lesion mapping of cognitive control and value-based decision making in the prefrontal cortex. *Proc Natl Acad Sci U S A*. 2012; 109:14681–14686. [PubMed: 22908286]
- Goldman-Rakic PS. Development of cortical circuitry and cognitive function. *Child Dev*. 1987; 58:601–622. [PubMed: 3608641]
- Gusnard DA, Akbudak E, Shulman GL, Raichle ME. Medial prefrontal cortex and self-referential mental activity: Relation to a default mode of brain function. *Proc Natl Acad Sci U S A*. 2001; 98:4259–4264. [PubMed: 11259662]
- Gusnard DA, Raichle ME. Searching for a baseline: functional imaging and the resting human brain. *Nat Rev Neurosci*. 2001; 2:685–694. [PubMed: 11584306]
- Hagmann P, Cammoun L, Gigandet X, Meuli R, Honey CJ, Wedeen VJ, Sporns O. Mapping the structural core of human cerebral cortex. *PLoS Biol*. 2008; 6:e159. [PubMed: 18597554]
- Harker KT, Whishaw IQ. A reaffirmation of the retrosplenial contribution to rodent navigation: reviewing the influences of lesion, strain, and task. *Neurosci Biobehav Rev*. 2004; 28:485–496. [PubMed: 15465136]
- Harley CA, Bielajew CH. A comparison of glycogen phosphorylase a and cytochrome oxidase histochemical staining in rat brain. *J Comp Neurol*. 1992; 322:377–389. [PubMed: 1325486]
- Hartigan JA, Wong MA. A k-means clustering algorithm. *Appl Stat*. 1979; 28:100–108.
- Hastie, T.; Tibshirani, R.; Friedman, J. *The Elements of Statistical Learning*. Springer Series in Statistics; Heidelberg, Germany: 2011.
- Hayden BY, Nair AC, McCoy AN, Platt ML. Posterior cingulate cortex mediates outcome-contingent allocation of behavior. *Neuron*. 2008; 60:19–25. [PubMed: 18940585]
- Hayden BY, Smith DV, Platt ML. Electrophysiological correlates of default-mode processing in macaque posterior cingulate cortex. *Proc Natl Acad Sci U S A*. 2009; 106:5948–5953. [PubMed: 19293382]
- Hensel L, Bzdok D, Müller VI, Zilles K, Eickhoff SB. Neural correlates of explicit social judgments on vocal stimuli. *Cereb Cortex*. in press.
- Holmes CJ, Hoge R, Collins L, Woods R, Toga AW, Evans AC. Enhancement of MR images using registration for signal averaging. *J Comput Assist Tomogr*. 1998; 22:324–333. [PubMed: 9530404]
- Ingvar DH. "Hyperfrontal" distribution of the cerebral grey matter flow in resting wakefulness; on the functional anatomy of the conscious state. *Acta Neurol Scand*. 1979; 60:12–25. [PubMed: 495039]
- Inoue K, Kawashima R, Satoh K, Kinomura S, Goto R, Koyama M, Sugiura M, Ito M, Fukuda H. PET study of pointing with visual feedback of moving hands. *J Neurophysiol*. 1998; 79:117–125. [PubMed: 9425182]
- Jakobs O, Langner R, Caspers S, Roski C, Cieslik EC, Zilles K, Laird AR, Fox PT, Eickhoff SB. Across-study and within-subject functional connectivity of a right temporo-parietal junction subregion involved in stimulus-context integration. *Neuroimage*. 2012; 60:2389–2398. [PubMed: 22387170]
- James, W. *The Principles of Psychology*. Henry Holt and Company; New York: 1890.

- Johansen-Berg H, Behrens TE, Robson MD, Drobnyak I, Rushworth MF, Brady JM, Smith SM, Higham DJ, Matthews PM. Changes in connectivity profiles define functionally distinct regions in human medial frontal cortex. *Proc Natl Acad Sci U S A*. 2004; 101:13335–13340. [PubMed: 15340158]
- Johnson SC, Baxter LC, Wilder LS, Pipe JG, Heiserman JE, Prigatano GP. Neural correlates of self-reflection. *Brain*. 2002; 125:1808–1814. [PubMed: 12135971]
- Kahnt T, Chang LJ, Park SQ, Heinzle J, Haynes JD. Connectivity-based parcellation of the human orbitofrontal cortex. *J Neurosci*. 2012; 32:6240–6250. [PubMed: 22553030]
- Kaufman, L.; Rousseeuw, PJ. *Finding Groups in Data: An Introduction to Cluster Analysis*. New York: 1990.
- Kelly C, Biswal BB, Craddock RC, Castellanos FX, Milham MP. Characterizing variation in the functional connectome: promise and pitfalls. *Trends Cogn Sci*. 2012; 16:181–188. [PubMed: 22341211]
- Kelly C, Uddin LQ, Shehzad Z, Margulies DS, Castellanos FX, Milham MP, Petrides M. Broca's region: linking human brain functional connectivity data and non-human primate tracing anatomy studies. *Eur J Neurosci*. 2010; 32:383–398. [PubMed: 20662902]
- Kircher TT, Senior C, Phillips ML, Rabe-Hesketh S, Benson PJ, Bullmore ET, Brammer M, Simmons A, Bartels M, David AS. Recognizing one's own face. *Cognition*. 2001; 78:B1–B15. [PubMed: 11062324]
- Klin A, Jones W, Schultz R, Volkmar F, Cohen D. Visual fixation patterns during viewing of naturalistic social situations as predictors of social competence in individuals with autism. *Arch Gen Psychiatry*. 2002; 59:809–816. [PubMed: 12215080]
- Kobayashi Y, Amaral DG. Macaque monkey retrosplenial cortex: I. three-dimensional and cytoarchitectonic organization. *J Comp Neurol*. 2000; 426:339–365. [PubMed: 10992242]
- Kobayashi Y, Amaral DG. Macaque monkey retrosplenial cortex: II. Cortical afferents. *J Comp Neurol*. 2003; 466:48–79. [PubMed: 14515240]
- Kobayashi Y, Amaral DG. Macaque monkey retrosplenial cortex: III. Cortical efferents. *J Comp Neurol*. 2007; 502:810–833. [PubMed: 17436282]
- Koster-Hale J, Saxe R. Theory of mind: a neural prediction problem. *Neuron*. 2013; 79:836–848. [PubMed: 24012000]
- Krienen FM, Tu PC, Buckner RL. Clan mentality: evidence that the medial prefrontal cortex responds to close others. *J Neurosci*. 2010; 30:13906–13915. [PubMed: 20943931]
- Kringelbach ML, Rolls ET. The functional neuroanatomy of the human orbitofrontal cortex: evidence from neuroimaging and neuropsychology. *Prog Neurobiol*. 2004; 72:341–372. [PubMed: 15157726]
- Laird AR, Eickhoff SB, Fox PM, Uecker AM, Ray KL, Saenz JJ Jr, McKay DR, Bzdok D, Laird RW, Robinson JL, Turner JA, Turkeltaub PE, Lancaster JL, Fox PT. The BrainMap strategy for standardization, sharing, and meta-analysis of neuroimaging data. *BMC Res Notes*. 2011a; 4:349. [PubMed: 21906305]
- Laird AR, Eickhoff SB, Fox PM, Uecker AM, Ray KL, Saenz JJ Jr, McKay DR, Bzdok D, Laird RW, Robinson JL, Turner JA, Turkeltaub PE, Lancaster JL, Fox PT. The BrainMap Strategy for Standardization, Sharing, and Meta-Analysis of Neuroimaging Data. *BMC Res Notes*. 2011b; 4:349. [PubMed: 21906305]
- Laird AR, Eickhoff SB, Kurth F, Fox PM, Uecker AM, Turner JA, Robinson JL, Lancaster JL, Fox PT. ALE Meta-Analysis Workflows Via the Brainmap Database: Progress Towards A Probabilistic Functional Brain Atlas. *Front Neuroinformatics*. 2009a; 3:23.
- Laird AR, Eickhoff SB, Li K, Robin DA, Glahn DC, Fox PT. Investigating the functional heterogeneity of the default mode network using coordinate-based meta-analytic modeling. *J Neurosci*. 2009b; 29:14496–14505. [PubMed: 19923283]
- Langner R, Kellermann T, Eickhoff SB, Boers F, Chatterjee A, Willmes K, Sturm W. Staying responsive to the world: modality-specific and -nonspecific contributions to speeded auditory, tactile, and visual stimulus detection. *Hum Brain Mapp*. 2012; 33:398–418. [PubMed: 21438078]

- Laureys S, Goldman S, Phillips C, Van Bogaert P, Aerts J, Luxen A, Franck G, Maquet P. Impaired effective cortical connectivity in vegetative state: preliminary investigation using PET. *Neuroimage*. 1999; 9:377–382. [PubMed: 10191166]
- LeDoux J. The amygdala. *Curr Biol*. 2007; 17:R868–874. [PubMed: 17956742]
- Leech R, Braga R, Sharp DJ. Echoes of the brain within the posterior cingulate cortex. *J Neurosci*. 2012; 32:215–222. [PubMed: 22219283]
- Leech R, Sharp DJ. The role of the posterior cingulate cortex in cognition and disease. *Brain*. 2014; 137:12–32. [PubMed: 23869106]
- Lynch CJ, Uddin LQ, Supekar K, Khouzam A, Phillips J, Menon V. Default mode network in childhood autism: posteromedial cortex heterogeneity and relationship with social deficits. *Biol Psychiatry*. 2013; 74:212–219. [PubMed: 23375976]
- Maddock RJ. The retrosplenial cortex and emotion: new insights from functional neuroimaging of the human brain. *Trends Neurosci*. 1999; 22:310–316. [PubMed: 10370255]
- Maguire EA. The retrosplenial contribution to human navigation: a review of lesion and neuroimaging findings. *Scand J Psychol*. 2001; 42:225–238. [PubMed: 11501737]
- Maguire EA, Burgess N, Donnett JG, Frackowiak RS, Frith CD, O'Keefe J. Knowing where and getting there: a human navigation network. *Science*. 1998; 280:921–924. [PubMed: 9572740]
- Maguire EA, Frackowiak RS, Frith CD. Recalling routes around london: activation of the right hippocampus in taxi drivers. *J Neurosci*. 1997; 17:7103–7110. [PubMed: 9278544]
- Maquet P. Functional neuroimaging of normal human sleep by positron emission tomography. *J Sleep Res*. 2000; 9:207–231. [PubMed: 11012860]
- Margulies DS, Vincent JL, Kelly C, Lohmann G, Uddin LQ, Biswal BB, Villringer A, Castellanos FX, Milham MP, Petrides M. Precuneus shares intrinsic functional architecture in humans and monkeys. *Proc Natl Acad Sci U S A*. 2009; 106:20069–20074. [PubMed: 19903877]
- Mars RB, Jbabdi S, Sallet J, O'Reilly JX, Crosson PL, Olivier E, Noonan MP, Bergmann C, Mitchell AS, Baxter MG, Behrens TE, Johansen-Berg H, Tomassini V, Miller KL, Rushworth MF. Diffusion-weighted imaging tractography-based parcellation of the human parietal cortex and comparison with human and macaque resting-state functional connectivity. *J Neurosci*. 2011; 31:4087–4100. [PubMed: 21411650]
- Mars RB, Sallet J, Neubert FX, Rushworth MF. Connectivity profiles reveal the relationship between brain areas for social cognition in human and monkey temporoparietal cortex. *Proc Natl Acad Sci U S A*. 2013; 110:10806–10811. [PubMed: 23754406]
- Matsunami K, Kawashima T, Satake H. Mode of [14C] 2-deoxy-D-glucose uptake into retrosplenial cortex and other memory-related structures of the monkey during a delayed response. *Brain Res Bull*. 1989; 22:829–838. [PubMed: 2765943]
- McCoy AN, Platt ML. Risk-sensitive neurons in macaque posterior cingulate cortex. *Nat Neurosci*. 2005; 8:1220–1227. [PubMed: 16116449]
- McCurdy LY, Maniscalco B, Metcalfe J, Liu KY, de Lange FP, Lau H. Anatomical coupling between distinct metacognitive systems for memory and visual perception. *J Neurosci*. 2013; 33:1897–1906. [PubMed: 23365229]
- Meila M. Comparing clusterings – an information based distance. *J Multivar Anal*. 2007; 98:873–895.
- Mesulam MM. A cortical network for directed attention and unilateral neglect. *Ann Neurol*. 1981; 10:309–325. [PubMed: 7032417]
- Mesulam MM. From sensation to cognition. *Brain*. 1998; 121(Pt 6):1013–1052. [PubMed: 9648540]
- Meyer ML, Lieberman MD. Social working memory: neurocognitive networks and directions for future research. *Front Psychol*. 2012; 3:571. [PubMed: 23267340]
- Morecraft RJ, Van Hoesen GW. Cingulate input to the primary and supplementary motor cortices in the rhesus monkey: evidence for somatotopy in areas 24c and 23c. *J Comp Neurol*. 1992; 322:471–489. [PubMed: 1383283]
- Murphy K, Birn RM, Handwerker DA, Jones TB, Bandettini PA. The impact of global signal regression on resting state correlations: are anti-correlated networks introduced? *Neuroimage*. 2009; 44:893–905. [PubMed: 18976716]

- Nanetti L, Cerliani L, Gazzola V, Renken R, Keysers C. Group analyses of connectivity-based cortical parcellation using repeated k-means clustering. *Neuroimage*. 2009; 47:1666–1677. [PubMed: 19524682]
- Nelson SM, Cohen AL, Power JD, Wig GS, Miezin FM, Wheeler ME, Velanova K, Donaldson DI, Phillips JS, Schlaggar BL, Petersen SE. A parcellation scheme for human left lateral parietal cortex. *Neuron*. 2010; 67:156–170. [PubMed: 20624599]
- Nichols T, Brett M, Andersson J, Wager T, Poline JB. Valid conjunction inference with the minimum statistic. *Neuroimage*. 2005; 25:653–660. [PubMed: 15808966]
- Nickl-Jockschat T, Habel U, Maria Michel T, Manning J, Laird AR, Fox PT, Schneider F, Eickhoff SB. Brain structure anomalies in autism spectrum disorder—a meta-analysis of VBM studies using anatomic likelihood estimation. *Hum Brain Mapp*. 2012; 33:1470–1489. [PubMed: 21692142]
- Ochsner KN. The social-emotional processing stream: five core constructs and their translational potential for schizophrenia and beyond. *Biol Psychiatry*. 2008; 64:48–61. [PubMed: 18549876]
- Palomero-Gallagher N, Vogt BA, Mayberg HS, Schleicher A, Zilles K. Receptor architecture of human cingulate cortex: insights into the four-region neurobiological model. *Hum Brain Mapp*. 2009; 30:2336–2355. [PubMed: 19034899]
- Parker A, Gaffan D. The effect of anterior thalamic and cingulate cortex lesions on object-in-place memory in monkeys. *Neuropsychologia*. 1997; 35:1093–1102. [PubMed: 9256374]
- Parvizi J, Van Hoesen GW, Buckwalter J, Damasio A. Neural connections of the posteromedial cortex in the macaque. *Proc Natl Acad Sci U S A*. 2006; 103:1563–1568. [PubMed: 16432221]
- Pearson JM, Hayden BY, Raghavachari S, Platt ML. Neurons in posterior cingulate cortex signal exploratory decisions in a dynamic multioption choice task. *Curr Biol*. 2009; 19:1532–1537. [PubMed: 19733074]
- Pelphrey KA, Sasson NJ, Reznick JS, Paul G, Goldman BD, Piven J. Visual scanning of faces in autism. *J Autism Dev Disord*. 2002; 32:249–261. [PubMed: 12199131]
- Pessoa L. On the relationship between emotion and cognition. *Nat Rev Neurosci*. 2008; 9:148–158. [PubMed: 18209732]
- Pfefferbaum A, Chanraud S, Pitel AL, Muller-Oehring E, Shankaranarayanan A, Alsop DC, Rohlfing T, Sullivan EV. Cerebral blood flow in posterior cortical nodes of the default mode network decreases with task engagement but remains higher than in most brain regions. *Cereb Cortex*. 2011; 21:233–244. [PubMed: 20484322]
- Poldrack RA. Can cognitive processes be inferred from neuroimaging data? *Trends Cogn Sci*. 2006; 10:59–63. [PubMed: 16406760]
- Radua J, Mataix-Cols D. Voxel-wise meta-analysis of grey matter changes in obsessive-compulsive disorder. *Br J Psychiatry*. 2009; 195:393–402. [PubMed: 19880927]
- Reetz K, Dogan I, Rolfs A, Binkofski F, Schulz JB, Laird AR, Fox PT, Eickhoff SB. Investigating function and connectivity of morphometric findings - Exemplified on cerebellar atrophy in spinocerebellar ataxia 17 (SCA17). *Neuroimage*. 2012; 62:1354–1366. [PubMed: 22659444]
- Richer F, Martinez M, Robert M, Bouvier G, Saint-Hilaire JM. Stimulation of human somatosensory cortex: tactile and body displacement perceptions in medial regions. *Exp Brain Res*. 1993; 93:173–176. [PubMed: 8467887]
- Rizzolatti G, Matelli M. Two different streams form the dorsal visual system: anatomy and functions. *Exp Brain Res*. 2003; 153:146–157. [PubMed: 14610633]
- Rudge P, Warrington EK. Selective impairment of memory and visual perception in splenial tumours. *Brain*. 1991; 114(Pt 1B):349–360. [PubMed: 2004246]
- Schacter DL, Addis DR, Buckner RL. Remembering the past to imagine the future: the prospective brain. *Nat Rev Neurosci*. 2007; 8:657–661. [PubMed: 17700624]
- Schall JD, Morel A, King DJ, Bullier J. Topography of visual cortex connections with frontal eye field in macaque: convergence and segregation of processing streams. *J Neurosci*. 1995; 15:4464–4487. [PubMed: 7540675]
- Scheperjans F, Eickhoff SB, Homke L, Mohlberg H, Hermann K, Amunts K, Zilles K. Probabilistic maps, morphometry, and variability of cytoarchitectonic areas in the human superior parietal cortex. *Cereb Cortex*. 2008a; 18:2141–2157. [PubMed: 18245042]

- Scheperjans F, Hermann K, Eickhoff SB, Amunts K, Schleicher A, Zilles K. Observer-independent cytoarchitectonic mapping of the human superior parietal cortex. *Cereb Cortex*. 2008b; 18:846–867. [PubMed: 17644831]
- Schilbach L, Bzdok D, Timmermans B, Fox PT, Laird AR, Vogeley K, Eickhoff SB. Introspective Minds: Using ALE Meta-Analyses to Study Commonalities in the Neural Correlates of Emotional Processing, Social & Unconstrained Cognition. *PLoS One*. 2012; 7:e30920. [PubMed: 22319593]
- Schilbach L, Eickhoff SB, Rotarska-Jagiela A, Fink GR, Vogeley K. Minds at rest? Social cognition as the default mode of cognizing and its putative relationship to the “default system” of the brain. *Conscious Cogn*. 2008; 17:457–467. [PubMed: 18434197]
- Scoville WB, Milner B. Loss of recent memory after bilateral hippocampal lesions. *J Neurol Neurosurg Psychiatr*. 1957; 20:11–21. [PubMed: 13406589]
- Seghier ML. The Angular Gyrus: Multiple Functions and Multiple Subdivisions. *Neuroscientist*. 2013:43–61. [PubMed: 22547530]
- Shima K, Aya K, Mushiake H, Inase M, Aizawa H, Tanji J. Two movement-related foci in the primate cingulate cortex observed in signal-triggered and self-paced forelimb movements. *J Neurophysiol*. 1991; 65:188–202. [PubMed: 2016637]
- Spreng RN, Mar RA, Kim AS. The common neural basis of autobiographical memory, prospection, navigation, theory of mind, and the default mode: a quantitative meta-analysis. *J Cogn Neurosci*. 2009; 21:489–510. [PubMed: 18510452]
- Stephan KM, Fink GR, Passingham RE, Silbersweig D, Ceballos-Baumann AO, Frith CD, Frackowiak RS. Functional anatomy of the mental representation of upper extremity movements in healthy subjects. *J Neurophysiol*. 1995; 73:373–386. [PubMed: 7714579]
- Takahashi N, Kawamura M, Shiota J, Kasahata N, Hirayama K. Pure topographic disorientation due to right retrosplenial lesion. *Neurology*. 1997; 49:464–469. [PubMed: 9270578]
- Thier P, Andersen RA. Electrical microstimulation distinguishes distinct saccade-related areas in the posterior parietal cortex. *J Neurophysiol*. 1998; 80:1713–1735. [PubMed: 9772234]
- Turkeltaub PE, Eden GF, Jones KM, Zeffiro TA. Meta-analysis of the functional neuroanatomy of single-word reading: Method and validation. *Neuroimage*. 2002; 16:765–780. [PubMed: 12169260]
- Turkeltaub PE, Eickhoff SB, Laird AR, Fox M, Wiener M, Fox P. Minimizing within-experiment and within-group effects in Activation Likelihood Estimation meta-analyses. *Hum Brain Mapp*. 2012; 33:1–13. [PubMed: 21305667]
- Uddin LQ, Supekar K, Amin H, Rykhlevskaia E, Nguyen DA, Greicius MD, Menon V. Dissociable connectivity within human angular gyrus and intraparietal sulcus: evidence from functional and structural connectivity. *Cereb Cortex*. 2010; 20:2636–2646. [PubMed: 20154013]
- Ungerleider LG, Haxby JV. ‘What’ and ‘where’ in the human brain. *Curr Opin Neurobiol*. 1994; 4:157–165. [PubMed: 8038571]
- Ungerleider, LG.; Mishkin, M. Two cortical visual systems. In: Ingle, DJ.; Mansfield, RJW., editors. *Analysis of Visual Behavior*. MIT Press; Cambridge: 1982. p. 549-586.
- Valenstein E, Bowers D, Verfaellie M, Heilman KM, Day A, Watson RT. Retrosplenial amnesia. *Brain*. 1987; 110(Pt 6):1631–1646. [PubMed: 3427404]
- Valiquette C, McNamara TP. Different mental representations for place recognition and goal localization. *Psychon Bull Rev*. 2007; 14:676–680. [PubMed: 17972732]
- Vallar, G.; Perani, D. The anatomy of spatial neglect in humans. In: Jeannerod, M., editor. *Neurophysiological and neuropsychological aspects of spatial neglect*. Elsevier; New York: 1987. p. 235-258.
- Van Overwalle F. A dissociation between social mentalizing and general reasoning. *Neuroimage*. 2011; 54:1589–1599. [PubMed: 20869452]
- Vann SD, Aggleton JP. Extensive cytotoxic lesions of the rat retrosplenial cortex reveal consistent deficits on tasks that tax allocentric spatial memory. *Behav Neurosci*. 2002; 116:85–94. [PubMed: 11895186]
- Vann SD, Aggleton JP, Maguire EA. What does the retrosplenial cortex do? *Nat Rev Neurosci*. 2009; 10:792–803. [PubMed: 19812579]

- Vogt BA. Pain and emotion interactions in subregions of the cingulate gyrus. *Nat Rev Neurosci*. 2005; 6:533–544. [PubMed: 15995724]
- Vogt BA, Barbas H. Structure and Connections of the Cingulate Vocalization Region in the Rhesus Monkey. *The Physiological Control of Mammalian Vocalization*. 1988:203–225.
- Vogt BA, Berger GR, Derbyshire SW. Structural and functional dichotomy of human midcingulate cortex. *Eur J Neurosci*. 2003; 18:3134–3144. [PubMed: 14656310]
- Vogt BA, Finch DM, Olson CR. Functional heterogeneity in cingulate cortex: the anterior executive and posterior evaluative regions. *Cereb Cortex*. 1992; 2:435–443. [PubMed: 1477524]
- Vogt BA, Laureys S. Posterior cingulate, precuneal and retrosplenial cortices: cytology and components of the neural network correlates of consciousness. *Prog Brain Res*. 2005; 150:205–217. [PubMed: 16186025]
- Vogt BA, Pandya DN. Cingulate cortex of the rhesus monkey: II. Cortical afferents. *J Comp Neurol*. 1987; 262:271–289. [PubMed: 3624555]
- Vogt BA, Pandya DN, Rosene DL. Cingulate cortex of the rhesus monkey: I. Cytoarchitecture and thalamic afferents. *J Comp Neurol*. 1987; 262:256–270. [PubMed: 3624554]
- Vogt BA, Vogt L, Laureys S. Cytology and functionally correlated circuits of human posterior cingulate areas. *Neuroimage*. 2006; 29:452–466. [PubMed: 16140550]
- Vogt BA, Vogt LJ, Perl DP, Hof PR. Cytology of human caudomedial cingulate, retrosplenial, and caudal parahippocampal cortices. *J Comp Neurol*. 2001; 438:353–376. [PubMed: 11550177]
- von Bechterew W. Demonstration eines Gehirns mit Zerstörung der vorderen und inneren Teile der Hirnrinde beider Schläfenlappen. *Neurol Zentbl*. 1900; 19:990–991.
- Wager TD, Lindquist M, Kaplan L. Meta-analysis of functional neuroimaging data: current and future directions. *Soc Cogn Affect Neurosci*. 2007; 2:150–158. [PubMed: 18985131]
- Weissenbacher A, Kasess C, Gerstl F, Lanzenberger R, Moser E, Windischberger C. Correlations and anticorrelations in resting-state functional connectivity MRI: a quantitative comparison of preprocessing strategies. *Neuroimage*. 2009; 47:1408–1416. [PubMed: 19442749]
- Whitfield-Gabrieli S, Ford JM. Default mode network activity and connectivity in psychopathology. *Annu Rev Clin Psychol*. 2012; 8:49–76. [PubMed: 22224834]
- Yarkoni T, Poldrack RA, Nichols TE, Van Essen DC, Wager TD. Large-scale automated synthesis of human functional neuroimaging data. *Nat Methods*. 2011; 8:665–670. [PubMed: 21706013]
- Yoder RM, Clark BJ, Taube JS. Origins of landmark encoding in the brain. *Trends Neurosci*. 2011; 34:561–571. [PubMed: 21982585]
- Yomogida Y, Sugiura M, Akimoto Y, Miyauchi CM, Kawashima R. The neural basis of event simulation: an fMRI study. *PLoS One*. 2014; 9:e96534. [PubMed: 24789353]
- Zhang S, Li C. Functional connectivity mapping of the human precuneus by resting state fMRI. *Neuroimage*. 2012; 59:3548–3562. [PubMed: 22116037]
- Zhang Y, Fan L, Zhang Y, Wang J, Zhu M, Zhang Y, Yu C, Jiang T. Connectivity-based parcellation of the human posteromedial cortex. *Cereb Cortex*. 2014; 24:719–727. [PubMed: 23146967]
- Zilles K, Amunts K. Centenary of Brodmann's map--conception and fate. *Nat Rev Neurosci*. 2010; 11:139–145. [PubMed: 20046193]

Highlights

- Connectivity-based parcellation identified four distinct cortical modules
- The clusters related to processing attention, perspectives, object and space facets
- All clusters were connected to the default-mode network at rest, but not during task

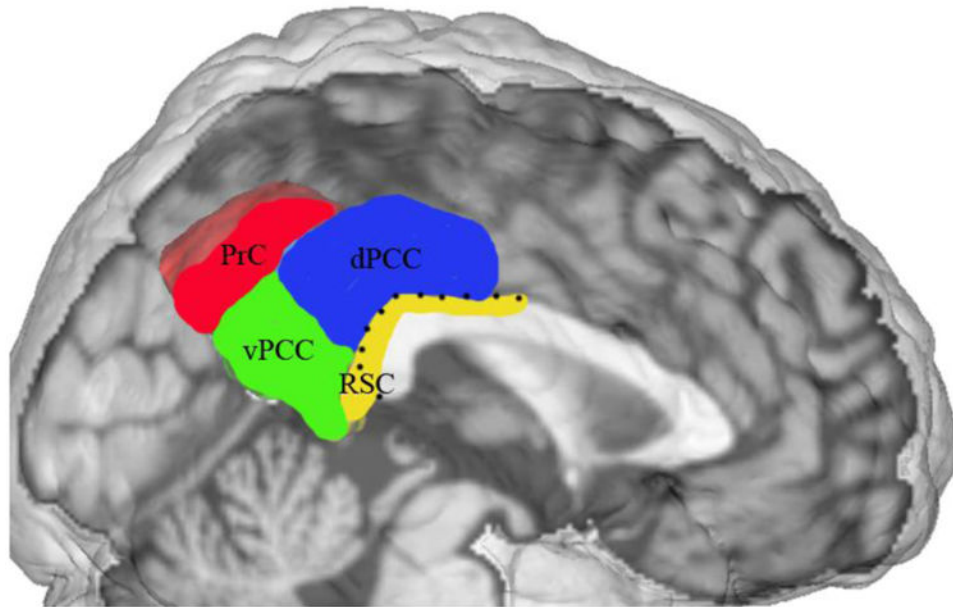


Figure 1. anatomy of the PMC

Sagittal slice of cerebral cortex with hand-drawn neuroanatomical model of the PMC. This figure was kindly provided by Brent A Vogt based on his previously published cytoarchitectonic investigations (2006, fig. 1). Notably, the RSC is bordered by a dotted line as it is frequently barely present on the medial cortical surface (cf. introduction). PrC = precuneus, vPCC = ventral posterior cingulate cortex, dPCC = dorsal posterior cingulate cortex, RSC = retrosplenial cortex.

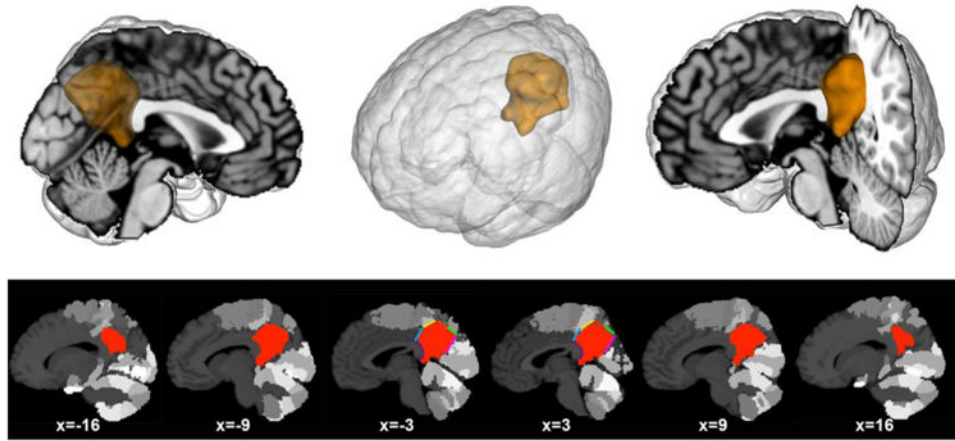


Figure 2. Location of the volume of interest in the PMC

The volume of interest (VOI) was created manually guided by bordering macroanatomical landmarks and cytoarchitectonic areas from the Jülich brain atlas (cf. method section). Our VOI comprised the posterior medial cortex providing the starting point for the present analyses. *Upper row*: the VOI was rendered on a T1-weighted MNI single-subject template using Mango (multi-image analysis GUI; <http://ric.uthscsa.edu/mango/>). *Lower row*: sagittal sections through the VOI based on the same template. Colors indicate anatomical borders that informed the VOI definition: blue (area 23d), yellow (5M), red (7A), green (7P), pink (parietooccipital sulcus), and purple (splenium of corpus callosum). The gray colored clusters of the brain template indicate cytoarchitectonic areas surrounding the VOI. Coordinates in MNI space.

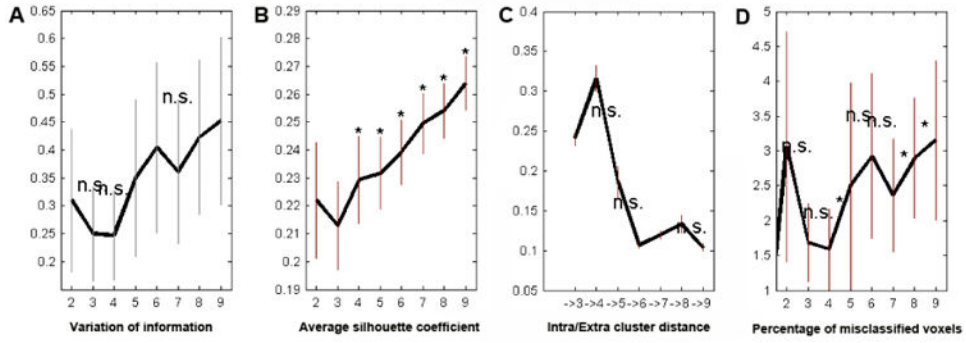


Figure 3. Different clustering criteria for model selection

Four different estimates of model fit advocated the superiority of the four-cluster solution. (A) Variation of information showed a decrease when moving from three to the four clusters and a considerable increase when moving from four to five clusters. (B) The silhouette exhibited a positive bump at four clusters in its upward trend starting from three clusters. (C) The change in the ratio of inter- versus intra-cluster distance was best at four clusters. (D) The percentage of misclassified voxels across filter sizes was lowest at four clusters. Thus, information-theoretic, cluster-separation, and topological criteria favored the four-cluster solution as the best fitting model given the data.

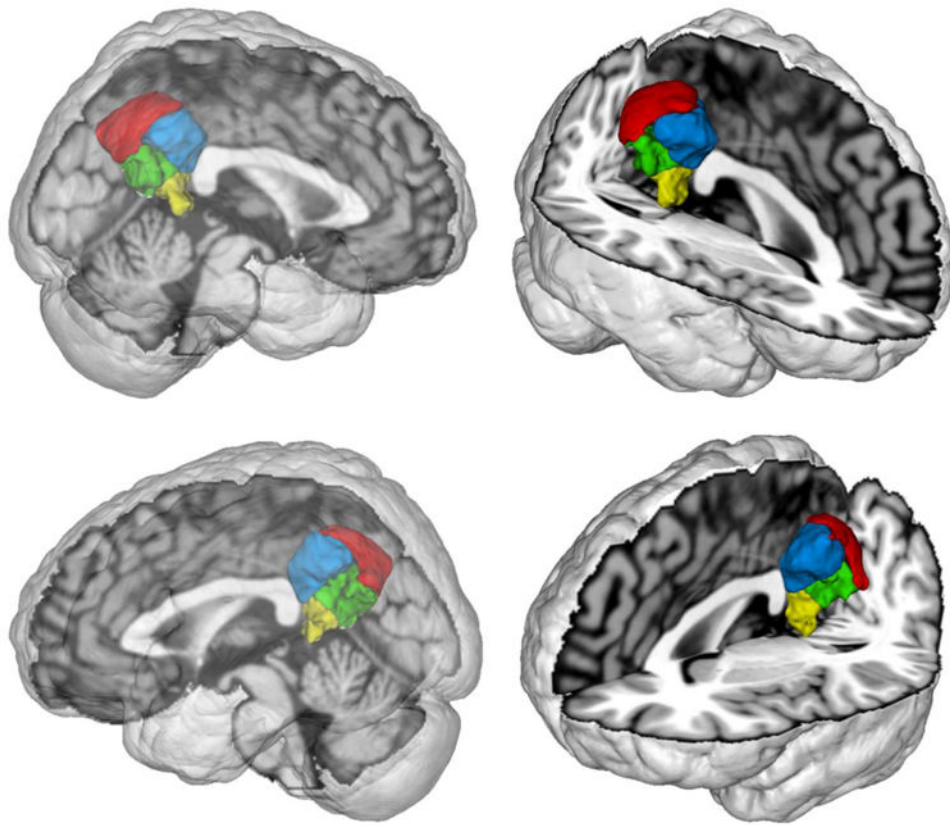


Figure 4. Connectivity-based parcellation results

Depicts the topographical decomposition of the volume of interest (Fig. 2) into four clusters of homogeneous connectivity. Red corresponds to precuneus (cluster 1), green corresponds to ventral posterior cingulate cortex (cluster 2), blue corresponds to dorsal posterior cingulate cortex (cluster 3), and yellow corresponds to retrosplenial cortex (cluster 4). Images were rendered using Mango.

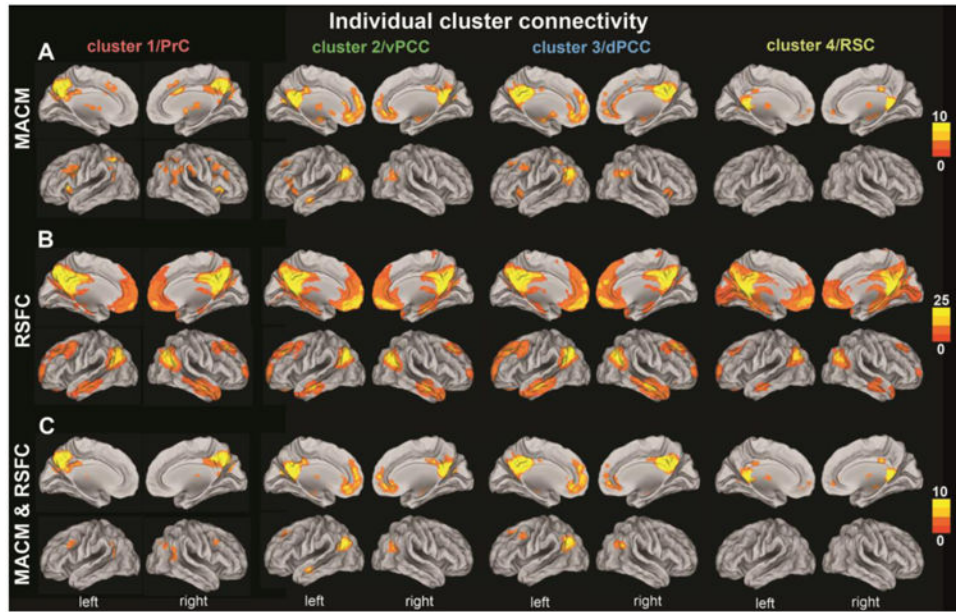


Figure 5. Connectivity profiles of the individual PMC clusters

Functional connectivity patterns of each cluster in the PMC VOI as individually determined using meta-analytic connectivity modeling (MACM; top two rows), resting-state functional connectivity (RSFC; middle two rows), and the conjunction of the results of both methods (MACM & RSFC; bottom two rows). The color bars on the right indicate z-values. All results survived a cluster-corrected threshold of $p < 0.05$ (i.e., corrected for multiple comparisons). All images were rendered on brain templates with inflated surfaces using Caret (computer assisted reconstruction and editing toolkit; <http://brainvis.wustl.edu/wiki/index.php/Caret>: About). PrC = precuneus, vPCC = ventral posterior cingulate cortex, dPCC = dorsal posterior cingulate cortex, RSC = retrosplenial cortex.

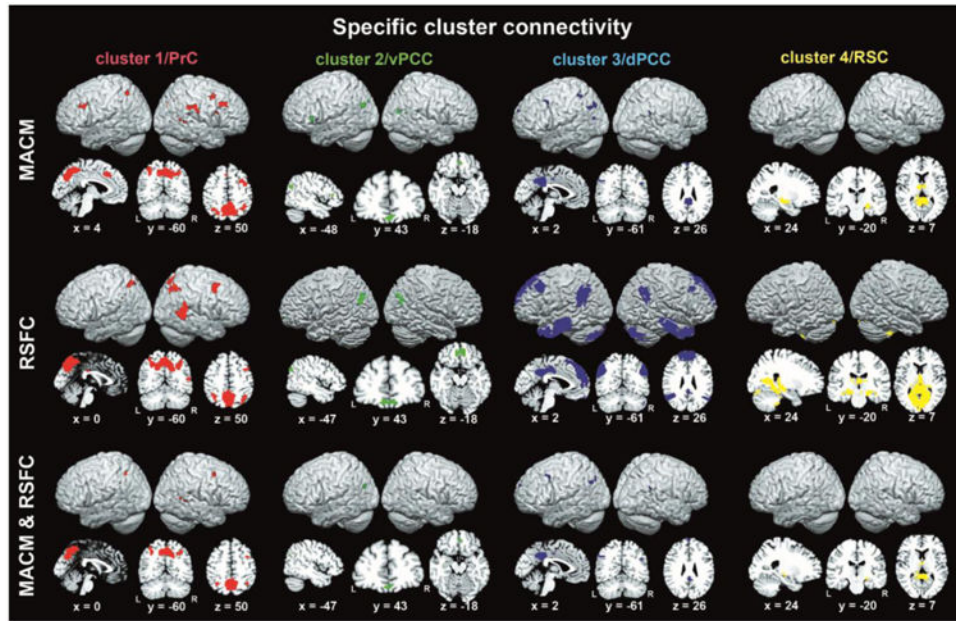


Figure 6. Specific connectivity profiles of the individual PMC clusters

Depicts renderings as well as sagittal, coronal, and axial section views of brain regions more strongly functionally connected to a given cluster than to any of the three other clusters according to meta-analytic connectivity modeling (MACM; top two rows), resting-state functional connectivity (RSFC; middle two rows), and the conjunction across MACM and RSFC (bottom two rows). Renderings and section views were created using MRICron (<http://www.mccauslandcenter.sc.edu/mricro/mricron/>) on a T1-weighted MNI single-subject template. Coordinates in MNI space. PrC = precuneus, vPCC = ventral posterior cingulate cortex, dPCC = dorsal posterior cingulate cortex, RSC = retrosplenial cortex.

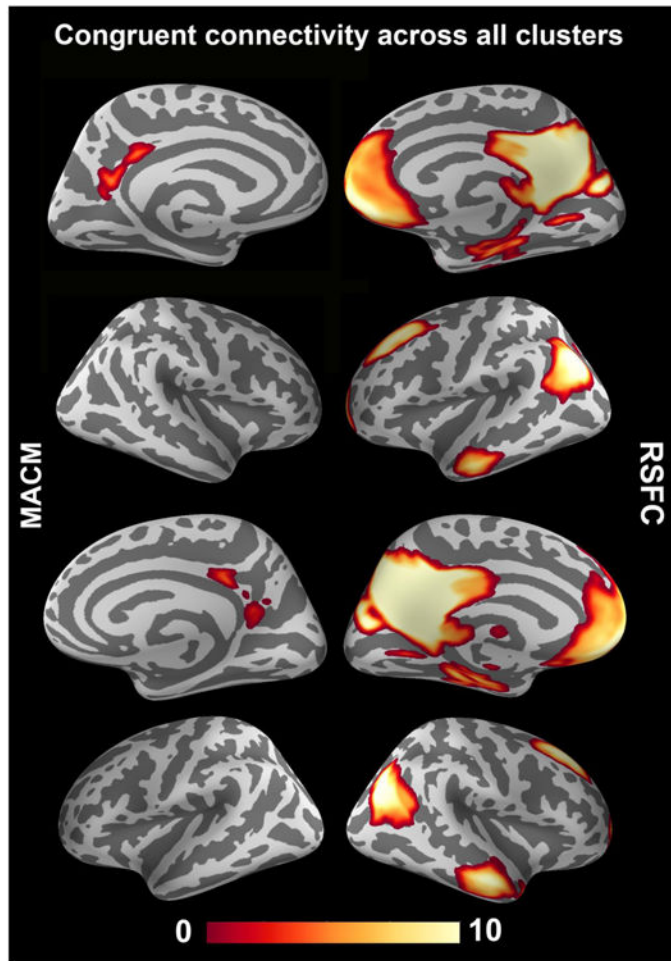


Figure 7. Congruent connectivity profiles across all PMC clusters

Depicts topographical overlap between the (cluster-level-corrected) whole-brain connectivity maps of the four PMC clusters (cf. Fig. 5). This AND conjunction was computed separately based on task-related meta-analytic connectivity modeling (MACM; left column) and task-unrelated resting-state functional connectivity (RSFC; right column) to quantify conjoint functional coupling of the PMC clusters across experimentally constrained (left column) and unconstrained (right column) brain states. The color bar on the bottom indicates z-values. Whole-brain renderings were created using PySurfer (<http://pysurfer.github.io/>).



Figure 8. Functional profiling of the PMC clusters

Significant associations with psychological terms from Behavioral *Domains* and *Paradigm* Classes of BrainMap meta-data (www.brainmap.org). Functional profiling was performed on each cluster individually. Forward inference determines above-chance brain activity given the presence of a psychological term, whereas reverse inference determines the above-chance probability of a psychological term given observed brain activity. All functional associations survived a significance threshold of $p < 0.05$. The x-axis indicates relative probability values. Bar plots were created using the ggplot2 package for R (<http://ggplot2.org/>). PrC = precuneus, vPCC = ventral posterior cingulate cortex, dPCC = dorsal posterior cingulate cortex, RSC = retrosplenial cortex.

Table 1

	Right IPC	Left IPC	Anterior RTPJ	Posterior RTPJ
Connectivity results (across MACM and RSFC)	Cytoarchitectonic coverage		#Voxel	
			450	540
Cluster 1 - individual			0	235
Cluster 1 - specific			0	23
Cluster 2 - individual	PGp (78%)	PGp (64%)	0	56
Cluster 2 - specific		PGp (100%)	0	3
Cluster 3 - individual	PGa (30%), PGp (50%)	PGa (29%), PGp (46%)	0	143
Cluster 3 - specific	PGp (63%)	PGa (78%)	0	5
Cluster 4 - individual			0	0
Cluster 4 - specific			0	0

Individual connectivity of the PMC subregions denotes the congruent findings of the cluster-level corrected MACM and RSFC results (Fig. 5, bottom row). *Specific* cluster connectivity of PMC subregions denotes the congruent maps of voxel more strongly connected to a given cluster than to all others across MACM and RSFC (Fig. 6, bottom row). All connectivity maps were based on cluster-level corrected inference (cf. methods section).

Left columns: Cytoarchitectonic assignment of significant connectivity clusters in the IPC (inferior parietal cortex) region (Caspers et al., 2006). The percentage indicates how many voxels of the significant connectivity findings were assigned to the respective cytoarchitectonic area. It is interesting to compare these results to previous connectivity analyses of PMC subregions (e.g., Mars et al., 2011; Nelson et al., 2010; Uddin et al., 2010).

Right column: The voxelwise definition of the previously reported anterior and posterior right temporo-parietal junction (RTPJ) (Bzdok et al., 2013b) has been quantitatively compared to the present cluster connectivity profiles. The indicated number reflects how many of these significant voxels are located to the anterior or posterior RTPJ cluster. Note that lack of parcellation of the left TPJ currently precludes comparison in the left hemisphere.